Article

Neuron

TDP-43 Depletion in Microglia Promotes Amyloid Clearance but Also Induces Synapse Loss

Highlights

- TDP-43 regulates microglial phagocytosis and clearance of Aβ
- Depletion of microglial TDP-43 results in enhanced synapse loss
- Depletion of microglial TDP-43 promotes amyloid clearance in a mouse model of AD
- TDP-43 pathology is associated with lower amyloid deposition in post-mortem brains

Authors

Rosa C. Paolicelli, Ali Jawaid, Christopher M. Henstridge, ..., Tara Spires-Jones, Paul E. Schulz, Lawrence Rajendran

Correspondence

rosachiara.paolicelli@irem.uzh.ch (R.C.P.), lawrence.rajendran@irem.uzh.ch (L.R.)

In Brief

Paolicelli et al. show that TDP-43 is a regulator of microglial phagocytosis. They found that mice lacking microglial TDP-43 display enhanced amyloid clearance but also significant synapse loss. They also show that TDP-43 pathology is associated with reduced amyloid burden in human brains.

Paolicelli et al., 2017, Neuron *95*, 297–308
July 19, 2017
http://dx.doi.org/10.1016/j.neuron.2017.05.037

CellPress

Neuron
Article

TDP-43 Depletion in Microglia Promotes Amyloid Clearance but Also Induces Synapse Loss

Rosa C. Paolicelli,[1,*] Ali Jawaid,[2] Christopher M. Henstridge,[3] Andrea Valeri,[1] Mario Merlini,[4] John L. Robinson,[5] Edward B. Lee,[5] Jamie Rose,[6] Stanley Appel,[7] Virginia M.-Y. Lee,[5] John Q. Trojanowski,[5] Tara Spires-Jones,[3] Paul E. Schulz,[8] and Lawrence Rajendran[1,9,*]

[1]Systems and Cell Biology of Neurodegeneration, IREM, University of Zurich, Schlieren, Switzerland
[2]Brain Research Institute, University of Zurich/ETH, Zurich, Switzerland
[3]Center for Cognitive and Neural Systems, University of Edinburgh, Edinburgh, UK
[4]Center for Molecular Cardiology - Vascular Aging & Stroke, University of Zurich, Schlieren, Switzerland
[5]Department of Pathology and Laboratory Medicine, University of Pennsylvania School of Medicine, Philadelphia, PA, USA
[6]Academic Neuropathology, Centre for Clinical Brain Sciences, University of Edinburgh, Edinburgh, UK
[7]ALS/MDA Center, The Methodist Hospital, Houston, TX, USA
[8]Department of Neurology, University of Texas, Health Science Center, Houston, TX, USA
[9]Lead Contact
*Correspondence: rosachiara.paolicelli@irem.uzh.ch (R.C.P.), lawrence.rajendran@irem.uzh.ch (L.R.)
http://dx.doi.org/10.1016/j.neuron.2017.05.037

SUMMARY

Microglia coordinate various functions in the central nervous system ranging from removing synaptic connections, to maintaining brain homeostasis by monitoring neuronal function, and clearing protein aggregates across the lifespan. Here we investigated whether increased microglial phagocytic activity that clears amyloid can also cause pathological synapse loss. We identified TDP-43, a DNA-RNA binding protein encoded by the *Tardbp* gene, as a strong regulator of microglial phagocytosis. Mice lacking TDP-43 in microglia exhibit reduced amyloid load in a model of Alzheimer's disease (AD) but at the same time display drastic synapse loss, even in the absence of amyloid. Clinical examination from TDP-43 pathology cases reveal a considerably reduced prevalence of AD and decreased amyloid pathology compared to age-matched healthy controls, confirming our experimental results. Overall, our data suggest that dysfunctional microglia might play a causative role in the pathogenesis of neurodegenerative disorders, critically modulating the early stages of cognitive decline.

INTRODUCTION

Microglia, the innate immune cells of the central nervous system (CNS), provide constant surveillance for neural functioning (Nimmerjahn et al., 2005; Davalos et al., 2005). They coordinate various critical roles throughout life, assisting early neuronal development and circuit formation and maintaining brain homeostasis (Paolicelli and Gross, 2011; Tremblay et al., 2011; Kettenmann et al., 2013). As the primary source of phagocytes in the CNS, microglia engulf cellular debris upon programmed apoptosis, remove excess synapses during neural circuit maturation, and clear the brain from potentially dangerous protein aggregates (Wakselman et al., 2008; Sierra et al., 2010; Lee and Landreth, 2010; Paolicelli et al., 2011; Prinz et al., 2011). Synapse elimination is activity dependent and strictly confined to the first postnatal weeks in the rodent brain, a physiological process defined as synaptic pruning (Paolicelli et al., 2011; Schafer et al., 2012). However, recent studies indicate that this process re-activates in Alzheimer's disease (AD), in which amyloid promotes microglia-mediated removal of synapses (Hong et al., 2016). Synaptic loss, an early and highly predictive correlate of cognitive decline (Terry et al., 1991), occurs not only in AD but also in other distinct neurodegenerative disorders characterized by the presence of toxic protein aggregates. This accumulation classifies these disorders as proteinopathies.

Evidence from genome-wide association studies (GWASs) reveals that most genes associated with risk to develop such disorders are highly expressed in microglia, which implies that they could modulate immune and phagocytic functions in disease states (Derecki et al., 2014). This hypothesis suggests that they may confer susceptibility to develop the diseases by modulating microglia-mediated protein aggregates clearance rather than production. We previously demonstrated that risk genes associated with late-onset AD do not affect amyloid production, which suggests that these predisposing genetic factors contribute to disease development through different mechanisms (Bali et al., 2012). These data implicate microglia in the pathogenesis of neurodegenerative disorders. However, it remains unknown whether an intrinsic dysfunction in microglia can promote pathological synaptic pruning leading to abnormal synapse loss.

RESULTS

TDP-43 Regulates Microglial Phagocytosis and Clearance of Aβ

Microglia, the scavenger cells of the brain, play a key role as moderators of protein aggregates clearance, which occurs

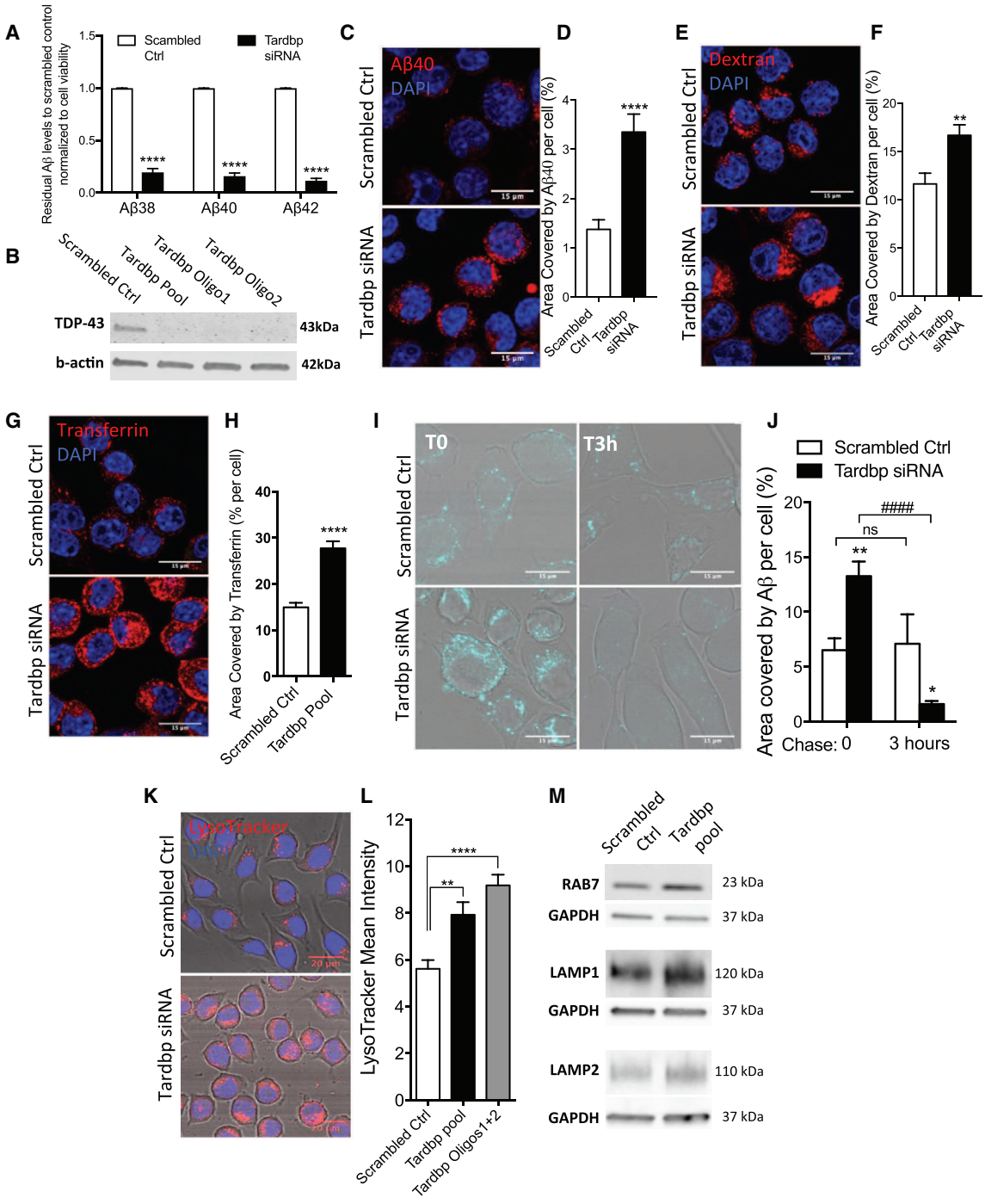

Figure 1. TDP-43 Loss Promotes Amyloid Phagocytosis and Degradation and Enhances Lysosomal Biogenesis in BV2 Microglia Cells

(A) Residual Aβ38, Aβ40, and Aβ42 levels from HeLa swAPP-conditioned medium, after overnight incubation with BV2 cells depleted of TDP-43, normalized to scrambled control and to cell viability (means ± SEM from three independent experiments, ****$p < 0.0001$, multiple unpaired t test).

(B) Western blot confirming the knockdown efficiency of Tardbp pool and single siRNA oligos in BV2 cells compared to scrambled control.

(C–H) Representative confocal micrograph (C) and relative quantification of BV2 cells uptaking fluorescently labeled Aβ40 (D) (scrambled control, n = 171 and Tardbp siRNA n = 147 BV2 cells); (E and F) dextran (control n = 47, Tardbp siRNA n = 47 cells) and (G and H) transferrin (control n = 68, Tardbp siRNA n = 68 cells); **$p < 0.005$, ****$p < 0.0001$ using two-tailed unpaired t test.

(I and J) Representative confocal images of scrambled control and Tardbp knockdown BV2 cells (I), with relative quantification soon after (T0, control n = 23; Tardbp siRNA n = 35 cells) and 3 hr (T3 hr, control n = 13; Tardbp n = 27 cells) after 60 min incubation with 1 μM Aβ40 (J). Values are shown as mean ± SEM,

(legend continued on next page)

intracellularly through enzymatic degradation following phagocytosis or extracellularly through degradation by secreted enzymes (Vekrellis et al., 2000; Nakanishi, 2003; Ries and Sastre, 2016; Solé-Domènech et al., 2016). We selected 18 top-ranked genes associated with neurodegenerative diseases and, using a loss-of-function approach, we screened them for their role to modulate microglial clearance of beta amyloid (Aβ), a well-established target for microglial phagocytosis and degradation (Paresce et al., 1996; Frenkel et al., 2013). Among the candidates we tested, TDP-43 exhibited the strongest Aβ clearance in BV2 cells, i.e., residual Aβ peptide levels measured from medium containing endogenous murine Aβ showed a significant reduction after exposure to cells in which TDP-43 gene was knocked down (Figures S1A–S1D).

TDP-43 is a 43 kDa DNA-RNA binding protein encoded by the *Tardbp* gene and is a known transcriptional repressor, mRNA binding protein, and splicing factor (Buratti and Baralle, 2001; Lagier-Tourenne et al., 2010; Polymenidou et al., 2011; Baralle et al., 2013). Ubiquinated TDP-43 aggregates represent the predominant constituent of cytoplasmic inclusions in glia and neurons in frontotemporal lobar degeneration (FTLD) and amyotrophic lateral sclerosis (ALS) patients, who show severe neuronal loss in frontal or motor cortex, respectively (Neumann et al., 2006). In the last years, the number of neurodegenerative disorders associated with TDP-43 pathology has considerably increased (Cook et al., 2008; Buratti and Baralle, 2009). The accompanying cell death in these disorders may arise from a combination of a toxic gain of function and a loss of nuclear TDP-43, both of which are associated with the presence of cytoplasmic aggregates (Cohen et al., 2011; Gendron and Petrucelli, 2011). Although a gain of toxicity induced by cytoplasmic inclusions can significantly contribute to the pathology (Xu et al., 2011; Medina et al., 2014; Walker et al., 2015), TDP-43 loss of function in neurons has been shown to be sufficient for inducing neuronal loss, accompanied by neuropathological alterations (Kraemer et al., 2010; Wu et al., 2012; Iguchi et al., 2013; Vanden Broeck et al., 2013). However, no evidence so far existed to support a role for loss of TDP-43 in microglia in the pathogenesis of the disease.

We wanted to confirm whether the enhanced clearance observed upon *Tardbp* knockdown could be also replicated with human Aβ. To this end, TDP-43-depleted BV2 cells were incubated overnight with conditioned medium derived from HeLa cells overexpressing the Swedish mutation of the human Amyloid Precursor Protein (sweAPP). This assay ensured that BV2 cells were exposed to medium containing high levels of human Aβ. Consistent with our findings from the murine Aβ screen, TDP-43 depletion resulted in a higher clearance capacity of all the Aβ species measured, compared to a scrambled control (Figure 1A). We achieved efficient TDP-43 depletion using either siRNA pools or single oligos (Figure 1B), with consistent results on amyloid clearance (Figure S1E).

To determine whether enhanced phagocytosis was the mechanism that mediated this enhanced clearance, we measured the internalization of fluorescently labeled Aβ peptide, a cargo previously reported to be phagocytosed by microglia (Paresce et al., 1996). In a validation experiment, the internalization of the Aβ peptide was followed in time lapse with the pH-dependent LysoTracker dye, to ensure that the cargo was trafficked to intracellular acidic compartments (Movie S1; Figurea S2A and S2B). TDP-43 depletion significantly enhanced intracellular levels of fluorescent Aβ (Figures 1C and 1D). Consistent with the enhanced uptake, we found a similar effect using fluorescently labeled dextran (Figures 1E and 1F) and transferrin (Figures 1G and 1H), which target uptake-mediated cargo. These results indicate that TDP-43 depletion in microglia increases the overall phagocytic activity.

Next, we determined whether the increased uptake was functionally followed by enhanced intracellular degradation. For that, we quantified the fluorescent signal of internalized Aβ40 3 hr after the uptake (T = 3 hr) and found a significant reduction in intracellular fluorescence, despite a higher uptake as measured by the initial amount (T = 0 hr) (Figures 1I and 1J). Since TDP-43 depletion increased intracellular degradation and amyloid is sorted to the lysosomal compartment for degradation in microglia (Cole et al., 1992), we examined whether increased lysosomal function occurs after TDP-43 depletion. We found higher levels of acidic late endosomal/lysosomal structures indicated by the pH-sensitive LysoTracker staining (Figures 1K and 1L). In addition, increased levels of lysosomal markers, such as LAMP1 and LAMP2, also accompanied the increased changes in acidic organelles in both BV2 cells (Figure 1M) and primary microglia cultures depleted of TDP-43 (Figures S3A–S3C). TDP-43 loss was recently shown to promote the nuclear translocation of TFEB, a transcription factor regulating lysosomal biogenesis (Xia et al., 2016). To investigate whether this was the case in microglia cells depleted of TDP-43, we assessed a subset of CLEAR (coordinated lysosomal expression and regulation) genes transcripts, downstream of TFEB, by RT-PCR. We found that the expression of *Lamp1*, *CtsD*, *CtsB*, *Clcn7*, *vATP6v1h*, *Psap*, and *Psen2* in TDP-43-depleted cells was higher than in scrambled control (Figure S3D). Overall, these data identify and validate TDP-43 as a regulator of microglial phagocytosis and clearance of Aβ.

Conditional Microglial TDP-43 Depletion *In Vivo* Promotes Phagocytosis of Stereotactically Injected Aβ

We then determined the physiological relevance of these findings *in vivo* by generating a microglial-specific inducible conditional TDP-43 knockout mouse line (cKO). We crossed mice expressing tamoxifen-inducible CRE recombinase (CreER) under the control of the endogenous Cx3cr1 microglia-specific promoter (Cx3cr1$^{creER-YFP}$; Parkhurst et al., 2013) with

*p < 0.05, **p < 0.01 versus scrambled control; ####p < 0.0001 Tardbp siRNA-T3 hr versus Tardbp siRNA-T0, using two-way ANOVA, followed by Bonferroni multiple comparison test.

(K and L) Representative confocal images of LysoTracker staining (K) and relative mean intensity quantification in control (n = 33) and TDP-43-depleted BV2 cells using siRNA Tardbp pool oligos, n = 36 or siRNA best 2 oligos, n = 36 (L). Data are shown as mean ± SEM, **p < 0.01, ****p < 0.0001, using one-way ANOVA followed by Dunnett's post hoc test.

(M) Representative blots for late endosomal/lysosomal markers in control and Tardbp knockdown BV2 cells.

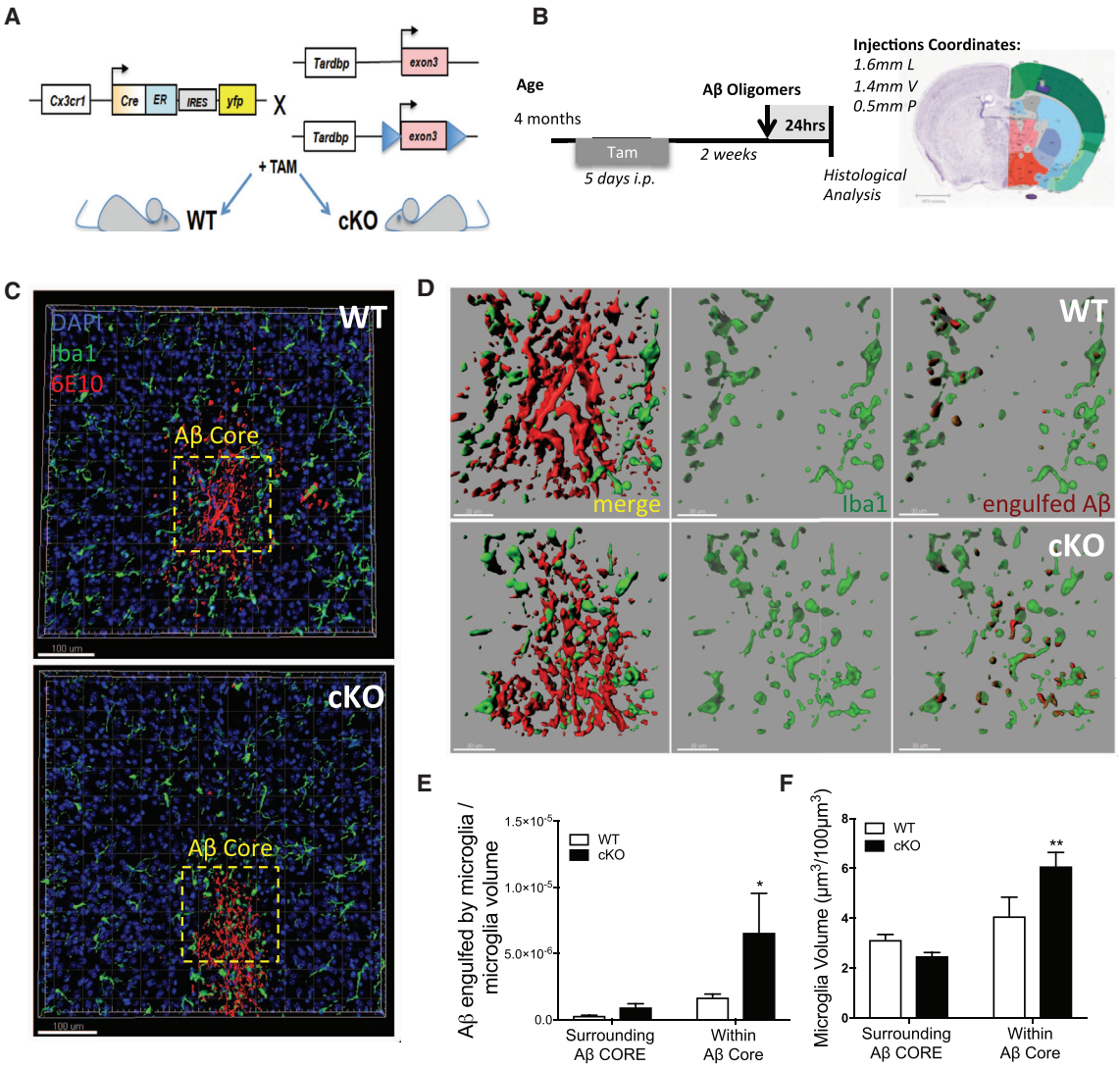

Figure 2. Inducible-Conditional Depletion of TDP-43 from Microglia Induces Enhanced Phagocytosis of Aβ42 Oligomers Administered by Stereotactic Injections

(A) Schematic representation of mouse breeding strategy for microglia-specific inducible conditional line, to obtain Cx3cr1^{CreER};Tardbp$^{+/+}$ (WT) and Cx3cr1^{CreER};Tardbp$^{floxed/floxed}$ (cKO) experimental subjects.

(B) Timeline for stereotactic injections of Aβ oligomers upon tamoxifen treatment in WT and cKO mice and relative coordinates of injections.

(C and D) 3D reconstruction of confocal stack acquisition in the somatosensory cortex of WT and cKO mice, 24 hr after the injection of 100 μM Aβ42 oligomers (C). Dashed-yellow frames enclosing Aβ core are zoomed in (D), showing a representative reconstruction of Iba1-positive microglia processes in green, surrounding (WT) or infiltrating (cKO) the 6E10-positive amyloid core in red. Increased engulfment of amyloid is appreciable in cKO microglia cells compared to WT controls.

(E and F) Quantification of microglia processes and Aβ engulfment surrounding or within amyloid core injection. Data are shown as mean ± SEM from WT, n = 8, and cKO, n = 7, stacks, acquired from n = 3 animals per genotype, *p < 0.05, **p < 0.01, using two-way ANOVA followed by uncorrected Fisher's LSD test.

Tardbp^{floxed} mice (Chiang et al., 2010) (Figure 2A). We confirmed that *Tardbp* transcript levels were significantly downregulated specifically in microglia isolated from cKO mice upon tamoxifen administration compared to WT controls, whereas overall cortical levels remained unchanged (Figures S4A and S4B). In addition, nuclear TDP-43 depletion was also confirmed at the protein level, in CRE-treated microglial primary cultures prepared from Tardbp^{floxed} mice (Figures S4C and S4D).

We then confirmed enhanced phagocytic uptake upon TDP-43 depletion *in vivo* by injecting Aβ42 oligomers in the cortex (100 μM, as prepared in Fa et al., 2010) and quantifying amyloid uptake 24 hr later (Figures 2B–2E). Interestingly, we observed a significant increase of microglia cells in close proximity to the amyloid core in cKO mice compared to WT littermates, whereas no differences occurred in the area surrounding the Aβ core (Figures 2D and 2F).

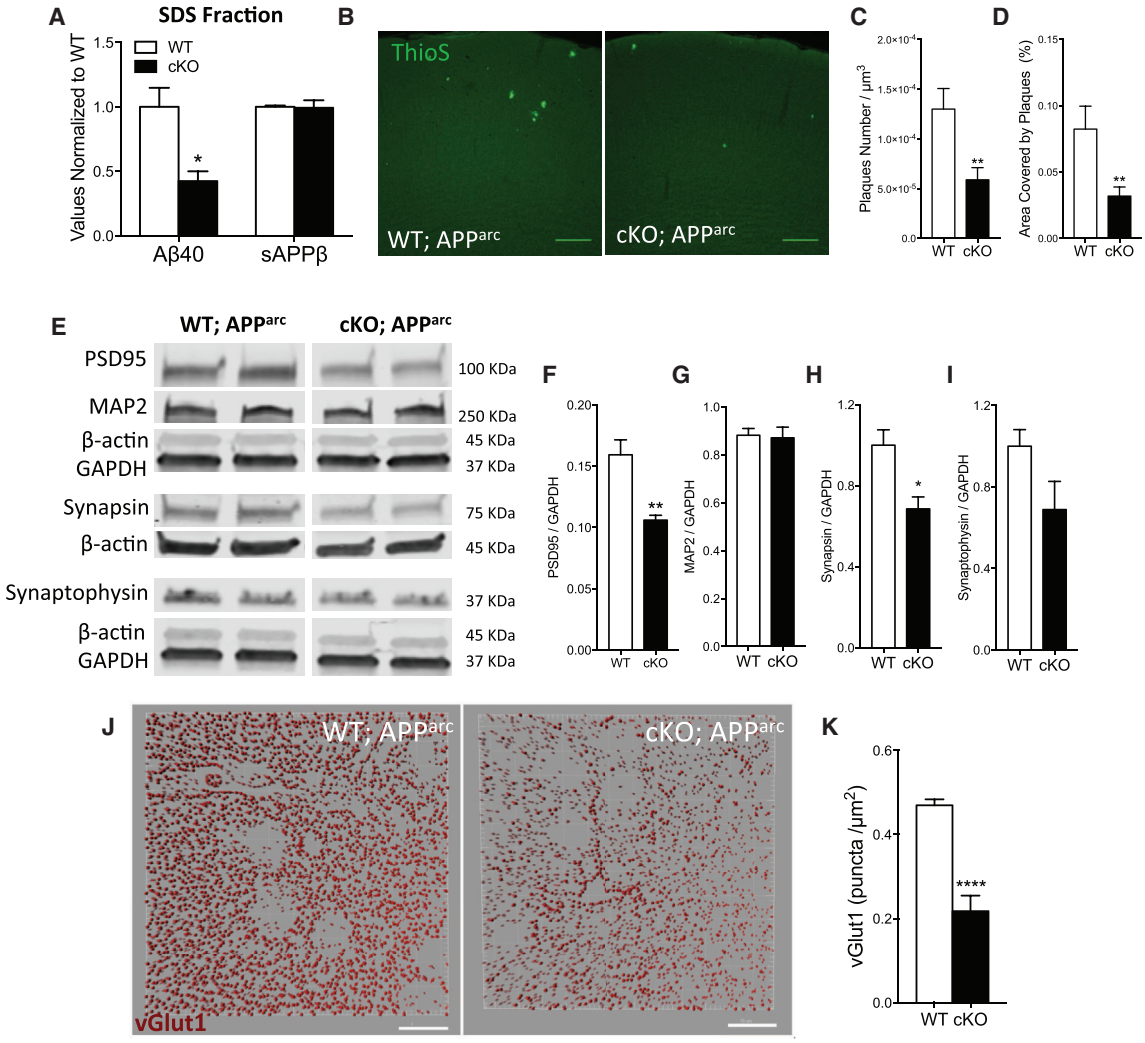

Figure 3. Depletion of TDP-43 from Microglia Enhances Amyloid Clearance but Exacerbates Synaptic Loss in a Mouse Model of AD

(A) Multiplexed electrocheminoluminescent assay measurements of Aβ40 and sAPPβ levels in the SDS-soluble fraction of cortex homogenates from 7-month-old APP^{arc} mice lacking TDP-43 in microglia. Mean ± SEM, n = 4 mice per genotype, **p < 0.01, using two-way ANOVA, followed by Sidak's post hoc test.

(B) Representative max-projections of confocal stacks from cortex of WT;APP^{arc} or cKO;APP^{arc} mice stained with Thioflavin S.

(C and D) Quantification of ThioS plaque density (C) and area covered by plaques from the cortex of 7-month-old APP^{arc}, WT (n = 36) and cKO (n = 36) with acquisitions from 4 animals per genotype (D). Mean ± SEM, **p < 0.01, using two-tailed unpaired t test.

(E–I) Representative blots for synaptic markers, from the cortex of 7-month-old APP^{arc} mice, WT or KO for microglial TDP-43 (E). Quantification of western blots for PSD95 (F), MAP2 (G), synapsin (H), and synaptophysin (I) normalized for GAPDH reference gene. Mean ± SEM, n = 4–5 mice per genotype, *p < 0.05, **p < 0.01, using two-tailed unpaired t test.

(J and K), Representative 3D reconstruction from confocal acquisitions of vGlut1 immunoreactivity in the cortex of WT and cKO mice (J) and relative quantification (K) (WT n = 25, cKO n = 17, acquisitions from 4 mice per genotype; ****p < 0.0001, two-tailed t test).

Conditional Depletion of Microglial TDP-43 Enhances Amyloid Clearance but Also Exacerbates Synaptic Loss in a Mouse Model of AD

In the light of all our findings indicating that TDP-43 depletion in microglia enhances the phagocytic uptake of Aβ, we hypothesized that this would promote clearance to reduce the total amyloid burden in a mouse model of AD. To this end, we crossed our Cx3cr1^{CreER};Tardbp^{floxed} mice with mice overexpressing human APP carrying the Arctic and Swedish mutations (APP^{arc}, Knobloch et al., 2007). Again, in this mouse model of AD, Aβ levels measurement revealed a significant reduction in cKO;APP^{arc} compared to WT;APP^{arc} littermates (Figure 3A) in the SDS fraction of brain homogenates and showed a similar trend in the TBS fraction (Figures S5A and S5B), confirming our *in vitro* results that TDP-43 depletion in microglia enhanced Aβ clearance. We found no differences in sAPPβ levels, a soluble intermediate product in the generation of Aβ, indicating that the amyloidogenic processing of APP was not affected, as also suggested by comparable levels of the full-length APP (Figure 3A; Figures S5A and S5C). These results definitely show

that TDP-43 depletion in microglia promotes Aβ clearance, rather than affecting production.

To investigate whether the enhanced Aβ clearance had any bearing on the amyloid load, we performed ThioS staining and observed a significant reduction in the cortex of cKO;APP^{arc} mice compared to WT (Figures 3B–3D), with no change in plaque size (Figure S5D). Levels of Iba1 and CD45 markers in microglia surrounding the plaques were comparable in cKO and WT controls (Figures S5E–S5G).

Since amyloid oligomers and plaques are considered the primary cause of synaptotoxicity in AD patients, we hypothesized that enhancing microglial-mediated amyloid clearance should preserve synapses. To our surprise, despite the reduction in amyloid load, we found a significant decrease in cortical synaptic markers in these mice as assayed by western blot (Figure 3E). Specifically, PSD95, a scaffold protein located in dendritic spines, was significantly reduced (Figure 3F), while levels of MAP2, a dendritic structural protein, were comparable between WT and cKO mice. These results suggest a specific reduction in dendritic spines rather than a general decrease in neuronal branches (Figure 3G). Consistently, levels of synapsin and synaptophysin were also reduced (Figures 3H and 3I). In addition, quantification of immunoreactive puncta for the synaptic marker vGlut1 also confirmed a drastic reduction in glutamatergic terminals (Figures 3J and 3K). These data show that microglia lacking TDP-43 can mediate enhanced removal and clearance of amyloid in an AD mouse model, but also in parallel, induce significant synapse loss. Overall these findings suggest that abnormally phagocytic microglia remove not only amyloid but also synapses.

In Vivo Depletion of TDP-43 from Microglia Results in Enhanced Synapse Loss Even in the Absence of Amyloid

Microglia are shown to re-activate synaptic pruning in the presence of Aβ oligomers (Hong et al., 2016). Since we observed synapse loss in mice depleted of microglial TDP-43 in APP transgenic model, we next asked whether amyloid is required for the synapse loss to occur.

To answer this question, we quantified the levels of synaptic markers in the cortex of WT and cKO mice where no human APP gene was overexpressed and thus no amyloid load was present. Here again, we found a significant decrease in vGlut1 and PSD95 (Figures 4A–4C). Since demyelination can occur in many neurodegenerative disorders, we also assayed levels of myelin-binding protein (MBP) isoforms and found a significant decrease (Figures 4A and 4D). The decrease in PSD95 was significant despite no changes in MAP2 levels, indicative of a selective synapse loss rather than general neuronal death (Figures 4A and 4E). Consistent with these findings, we observed a significant decrease in cortical dendritic spine density in cKO mice (Figures 4F and 4G). vGlut1 immunohistochemistry also revealed a significant decrease in mice depleted of microglial TDP-43 compared to controls (Figures 4H and 4I). These results conclusively show that synapse loss occurs due to microglial TDP-43 depletion in mice, independent of amyloid load.

To directly assess the role of microglia in synapse elimination in these mice, we quantified synapse engulfment through 3D reconstruction of confocal acquisitions. Since we observed synaptic immunoreactive puncta within CD68-positive phagocytic structures inside microglia cells (Figure S6), our signal co-localization was specific. We then quantified PSD95 immunoreactive puncta within and surrounding microglia cells. There was a significant increase in the fraction of synaptic marker engulfed by TDP-43 depleted microglia compared to WT controls (Figures 4J and 4K). We also observed a significant increase in the phagocytic marker CD68 (Figure 4L). The cells had increased size and total volume of CD68-positive structures, despite no change in number of structures (Figures 4M–4O). Overall, these data show that abnormal microglial phagocytosis induced by TDP-43 depletion mediates synapse loss, regardless of the presence of amyloid.

TDP-43 Pathology Is Associated with Lower Prevalence of AD and Higher Microglial Phagocytic Markers in Post-mortem Human Brains

In line with our findings, we predicted that enhanced microglia-mediated clearance would affect cognitive decline by targeting synapses yet simultaneously reducing amyloid plaque load. This dual function could complicate the diagnosis of AD, which has been a topic of discussion for a very long time—whether amyloid load correlates with the cognitive decline (Braak and Braak, 1998; Serrano-Pozo et al., 2011; Nelson et al., 2012). We evaluated the prevalence of AD in a large cohort (n = 698) of ALS patients that typically exhibit TDP-43 pathology (Table S1). We selected an age cutoff of 65 years or older, as individuals over the age of 65 are at increased risk of sporadic AD. The prevalence of AD in ALS patients aged 65 to 74 years was comparable to what is expected in the normal population (reference to Hebert et al., 2013); however, the AD prevalence was considerably lower in ALS patients aged 75 years and above (Figure 5A). Notably, cognitive evaluation revealed a subtle cognitive dysfunction in non-AD ALS patients older than 75 years, despite excluding patients with over-lapping FTLD (Figure 5B). These findings suggest that TDP-43 pathology is associated with reduced amyloid burden and may underlie subtle cognitive deficits in non-AD ALS patients. These clinical data support our overall hypothesis that dysfunctional microglia (as due to TDP-43 pathology) can mediate both enhanced amyloid clearance and synapse loss. This suggests that TDP-43 pathology might promote neurodegeneration through synapse loss on one hand, but on the other might also reduce the risk for enhancing the amyloid load and thus decrease the prevalence of AD.

To verify that the observed decreased prevalence of AD in ALS patients is secondary to decreased amyloid burden, we quantified amyloid pathology in an independent brain autopsy cohort, composed of healthy controls, AD cases, and TDP-43 cases (ALS and FTLD-TDP-43). The quantification of Aβ was performed using Thal Aβ phase (TAP) scoring system. TAP relies on immunohistochemistry and evaluates presence or absence of all Aβ plaques spatially across several neocortical, limbic, and subcortical regions of the brain. TAP staging is superior to other methods of Aβ quantification in its sensitivity for Aβ, as well as prediction of dementia symptoms (Boluda et al., 2014). Using TAP scoring, we observed Aβ plaque burden to be comparable to age-matched controls in 65- to 74-year-old ALS/FTLD-TDP patients. However, similar to how AD prevalence was lower in

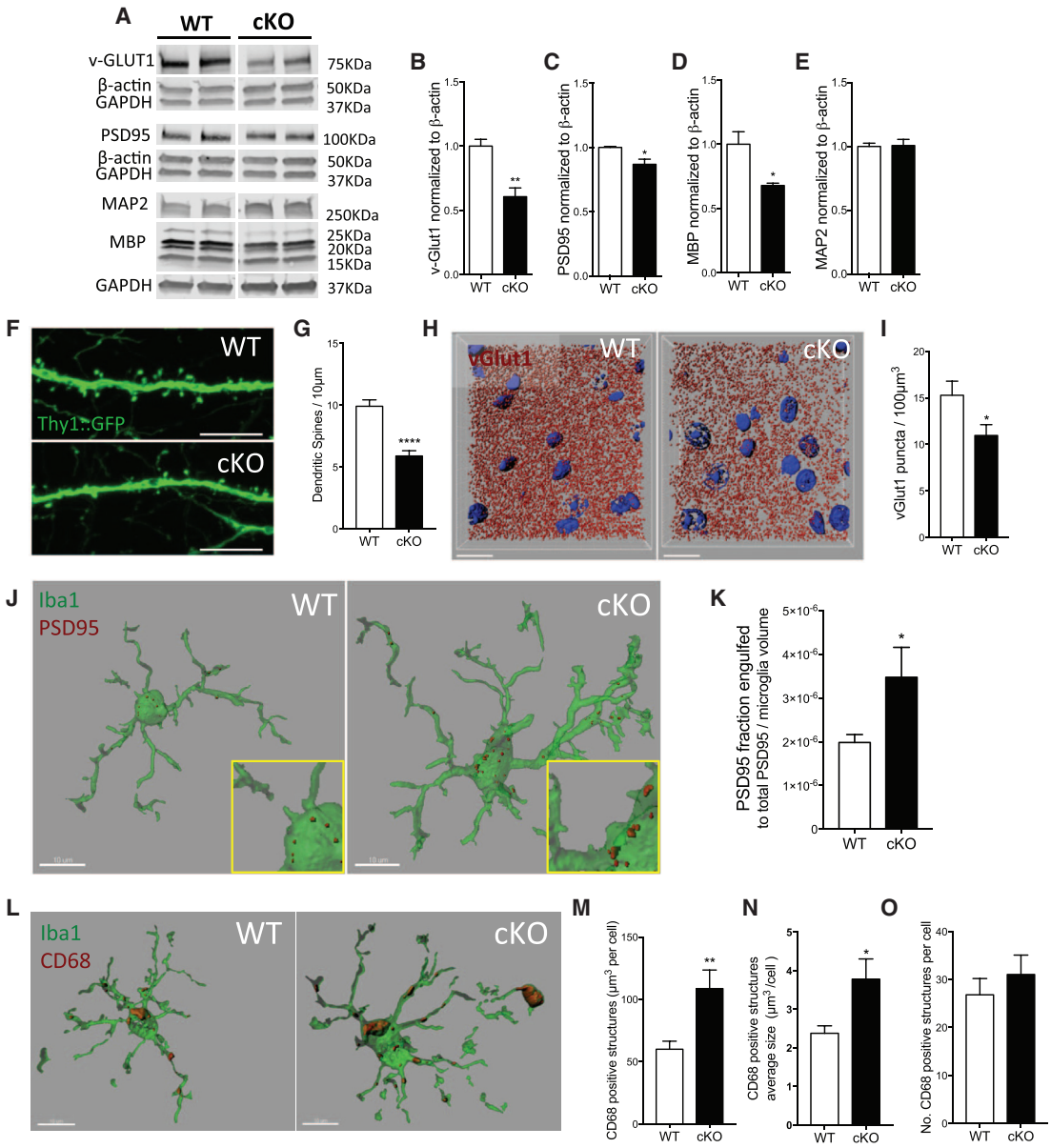

Figure 4. Selective Depletion of TDP-43 from Microglia Results in Enhanced Synaptic Loss in Mice Even in the Absence of Amyloid

(A–E) Representative blots of synaptic markers in the motor/somatosensory cortex of WT and cKO 8-month-old mice (A) and relative quantification for vGlut-1 (B), PSD95 (C), MBP (D), and MAP2 (E) normalized to β-actin reference gene. Mean ± SEM, n = 3–4 mice per genotype, *p < 0.05, **p < 0.01, unpaired two-tailed t test.

(F and G) Representative confocal micrograph of dendritic spines from motor/somatosensory cortex of WT and cKO mice (F) (scale bar: 10 μm), and relative quantification (G) (WT n = 53, cKO n = 47 segments, from 4 animals per genotype).

(H and I) Representative 3D reconstruction of vGlut1 immunoreactive puncta in the somatosensory cortex of WT and cKO mice (H) (scale bar: 15 μm), and relative quantification (I) (WT n = 8, cKO n = 10 acquisitions from 3 animals per genotype; *p < 0.05, using two-tailed t test).

(J and K) Representative 3D reconstruction of single microglia cells engulfing PSD95 (J) and quantified as fraction of engulfed PSD95 normalized to microglia volume (K) (means ± SEM, WT n = 12 and cKO n = 12 cells from 3 animals per genotype; *p < 0.05, using two-tailed t test).

(L–O) Representative 3D reconstructions showing CD68-positive structures within Iba1-microglia cells (L) (scale bar: 10 μm). Quantification of CD68 structures total volume per cell (M), average size per CD68-structure (N), and number of CD68-positive structures per cell (O) (WT n = 16 and cKO n = 20, from 3 animals per genotype).

ALS patients who were 75 years or older, Aβ pathology was significantly reduced in the brains collected from ALS/FTLD-TDP patients 75 years or older, compared to the age-matched controls (Figures 5C and 5D). These findings suggest that TDP-43 pathology might promote enhanced amyloid clearance and hence prevent against AD.

To further validate the increase in the microglial phagocytic marker CD68 observed in our mouse model, we examined an

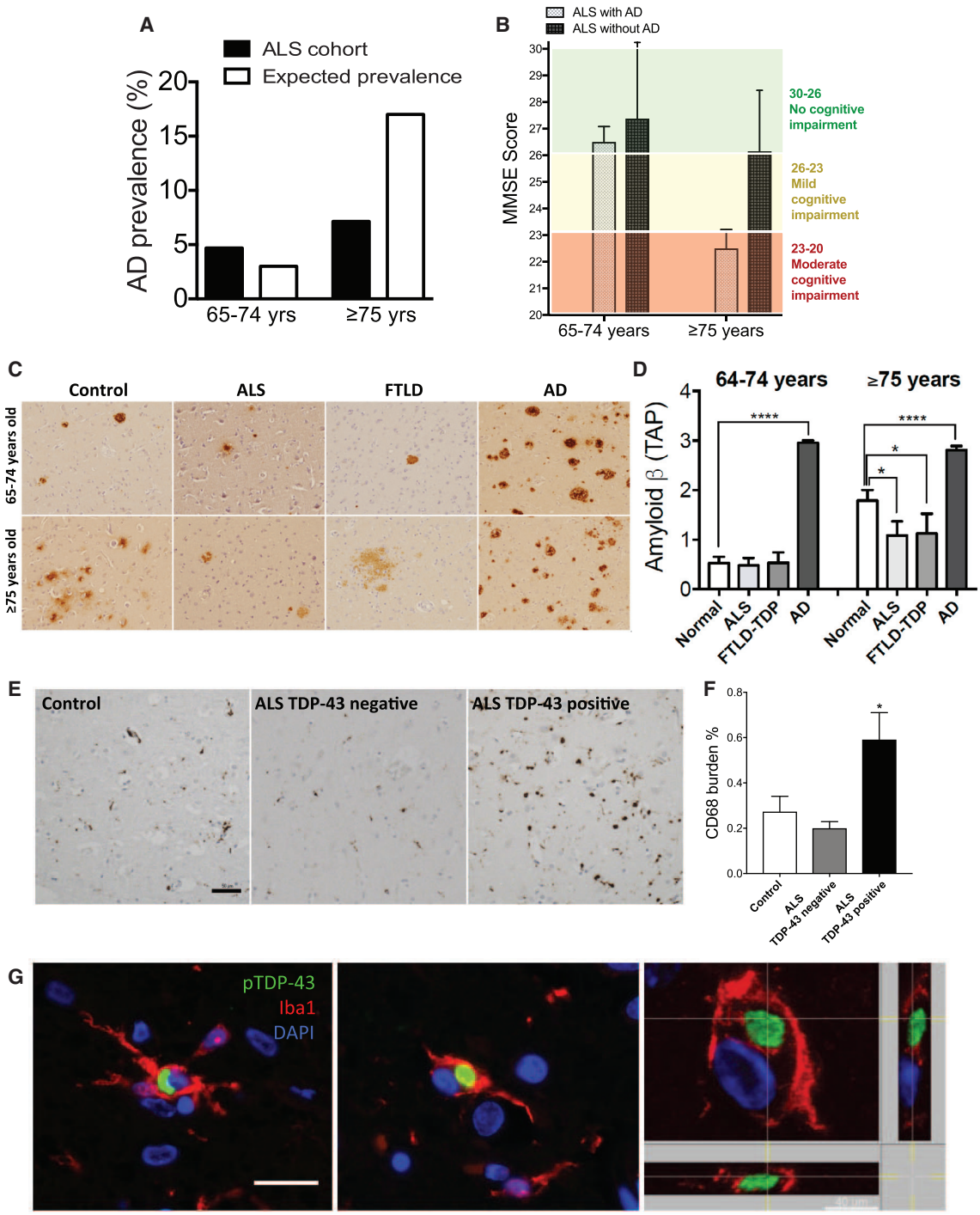

Figure 5. Prevalence of AD in ALS/FTLD Patients Is Significantly Lower than in Healthy Controls

(A) Prevalence of AD in ALS patients compared to expected prevalence in a normal age-matched population. ALS cohort was divided into two sub-groups according to their age at the time of AD screening: 65–74 and ≥75 years. The expected prevalence of AD in these age groups is 3% and 17%, respectively. AD prevalence is 4.7% in ALS patients aged 65–74 years but increases to only 7.1% in those ≥75 years.

(B) MiniMental State Examination (MMSE) scores reported from ALS patients with or without AD, indicate a mild cognitive impairment in ALS patients above 75, despite no AD.

(C) Representative images of beta-amyloid load in Control, ALS, FTLD, and AD biopsies in 65–74 and ≥75 years cases.

(D) Amyloid burden quantified according to the Thal Aβ phase (TAP) scoring system, in 65–74 and ≥75 years controls, ALS, FTLD, and AD cases indicates decreased Aβ in ALS and FTLD cases ≥75 years (mean ± SEM, Control n = 40, ALS n = 35, FTLD n = 25, AD n = 62, *p < 0.05, ****p < 0.0001, by one-way ANOVA of unpaired t test, followed by Holm-Sidak's multiple comparisons test).

(legend continued on next page)

independent brain autopsy cohort. To this end, we tested the levels of cortical CD68 in the context of ALS pathology. Importantly, we found that CD68 burden was significantly higher in ALS patients with TDP-43 pathology as compared to ALS patients without TDP-43 inclusions, or to healthy controls (Figures 5E and 5F; Table S2), supporting a critical role for TDP-43 in regulating microglial function. Finally, to assess the clinical relevance of the described microglial phenotype, we investigated whether TDP-43 aggregates could be found in the microglia of TDP-43 pathology cases. To this aim, we analyzed eight motor neurodegenerative (MND) cases with TDP-43 pathology and four healthy controls. In the MND cases, but not in the controls, we could observe examples of cytoplasmic inclusions positively stained for phospho-TDP-43 (pTDP-43) within microglial cells positive for Iba1 (Figure 5G), indicating that microglial TDP-43 can contribute to TDP-43 pathology. Importantly, though rare, pTDP-43 inclusions in microglia were found in all of the MND cases examined. Overall these findings corroborate the clinical relevance for a dysfunctional, abnormally phagocytic microglial phenotype in TDP-43 pathology.

DISCUSSION

Here we show that loss of TDP-43 in microglia enhances phagocytosis and amyloid clearance following acute Aβ oligomers injection and in a mouse model of AD. The abnormal phagocytosis induced by loss of TDP-43 concurrently resulted in an excessive loss of synapses independent of amyloid deposition. Our data demonstrate enhanced lysosomal function following TDP-43 depletion. However, further studies are now required to identify the exact mechanism through which TDP-43 regulates lysosome biogenesis and also enhanced phagocytosis. One possibility is that TDP-43 negatively controls lysosomal biogenesis genes such as the CLEAR genes that are regulated by the transcription factor TFEB. In this study, we found that TDP-43 depletion results in the increase transcription of genes related to lysosomal biogenesis; however, we focused only on a selected set of CLEAR genes. Whether TDP-43 regulates lysosome biogenesis through the entire CLEAR gene network needs to be further elucidated. Alternatively TDP-43 could also regulate mTOR activity, which in turn regulates lysosome biogenesis via the Raptor-TSC2-TFEB-lysosome/autophagosome biogenesis. Recent study performed in HeLa cells showed that TDP-43 loss promotes autophagosomal biogenesis as a direct consequence of decreased Raptor mRNA stability and promotes nuclear translocation of TFEB, a transcription factor master regulator of lysosomal genes (Ying et al., 2016). Our findings suggest that TDP-43 depletion positively regulates lysosomal genes downstream of TFEB. However, it remains to be tested whether TDP-43 loss leads to decreased Raptor mRNA and regulation of mTOR activity in microglia cells.

TDP-43 cytoplasmic inclusions can occur in multiple neurodegenerative diseases, which are collectively defined as TDP-43 proteinopathies. This classification highlights a key role for TDP-43 in the disease pathogenesis (Cohen et al., 2011). Previous studies indicate a causal role for TDP-43 neuronal pathology in the pathogenesis of neurodegeneration and synaptic loss using animal models of disease. These studies suggest, in fact, a cell-autonomous TDP-43 neurotoxicity (Igaz et al., 2011; Xu et al., 2011; Diaper et al., 2013; Yang et al., 2014; Medina et al., 2014; Handley et al., 2016).

Recent studies revealed additional non-autonomous functions for TDP-43 pathology in *Drosophila* glia, which result in defective synapses and axonal wrapping of motor neurons (Romano et al., 2015). However, neither a direct demonstration of microglial TDP-43 function nor its direct contribution to the pathological phenotype has been yet proposed. Here we provide evidence that phosphorylated TDP-43 aggregates can be found in the microglia of human post-mortem brains with TDP-43 pathology, thus opening the possibility that microglial TDP-43 might contribute to the pathogenesis of the disease.

In our model, a microglial-specific dysfunction induced by a loss of TDP-43 mediates a non-cell-autonomous neurotoxic effect, which could sum to other cellular phenotypes and critically contribute to the disorder. However, we cannot exclude the involvement of other Cx3cr1-positive non-parenchymal myeloid cells, considering that Cx3cr1-driven recombination also occurs in perivascular and meningeal macrophages (Goldmann et al., 2016).

Our data show that abnormal phagocytosis and clearance elicited in microglia following TDP-43 loss is ultimately paradoxical. These processes are not entirely beneficial in the context of a complex organism, since microglial phagocytic activity might not only enable clearance of protein aggregates but also synaptic connection loss. These mixed responses may underlie the failure of many AD drug treatment clinical trials to improve cognitive function, despite the progressive reductions in amyloid burden.

Synaptic pruning by microglia can re-activate in the presence of Aβ oligomers, since complement molecules upregulate in the disease state to ultimately mediate synapse removal (Hong et al., 2016). Here we show that an intrinsic dysregulation of microglia induced by TDP-43 depletion is sufficient to trigger abnormal synapse loss, even in the absence of Aβ oligomers. Our results further suggest that microglial dysfunction underlies the pathogenesis of many disparate and distinct neurodegenerative disorders. In line with our results, a recent study reported that selective neuronal depletion of TDP-43 was sufficient to reduce amyloid burden and to exacerbate cognitive deficits in an AD mouse model, suggesting that common mechanisms induced by loss of TDP-43 may partially explain the enhanced amyloid clearance (LaClair et al., 2016).

(E and F) Representative micrographs for immunostaining against CD68 in cortical section of healthy control, and ALS cases negative and positive for TDP-43 pathology, respectively (E). Relative quantification of CD68 burden in ALS patients with and without TDP-43 pathology indicates increased burden in ALS patients with TDP-43 pathology (F) (mean ± SEM, Control n = 6; *p < 0.05, ALS TDP-43 negative (n = 11) versus ALS TDP-43 positive (n = 16), by using two-tailed unpaired t test); scale bar: 50 μm.

(G) Representative confocal z stack and orthogonal projections of microglial cells positive for Iba1 and pTDP-43 markers, in human post-mortem cortical sections of MND cases; scale bar: 20 μm; scale bar for the orthogonal projection: 40 μm.

Consistent with our experimental findings, we show that the prevalence of AD was considerably reduced in a cohort of ALS patients when compared to the expected AD prevalence in the normal population. Nevertheless, these ALS patients without AD still exhibited a subtle decline in cognitive function, which suggests an underlying loss of synapses. Importantly, neuropathological examination of post-mortem human brains showed a significant reduction of amyloid burden in ALS/FTLD-TDP-43 cases, as compared to age-matched healthy controls. These findings suggest that TDP-43 pathology might lead to enhanced Aβ clearance and hence delay AD. However, in the same dataset, a comparison of Aβ levels within AD cases with or without TDP-43 pathology did not reveal any major difference. This observation could suggest that the enhanced clearance through TDP-43 pathology might modulate the initial stages of amyloid deposition, but have no effects once the amyloid burden has established. Further studies are required to better elucidate the correlation between AD and TDP-43 pathology.

Indeed, a recent study from a population-based sample revealed a strong association of TDP-43 inclusions with late-onset dementia, but not with AD markers of amyloid and tau (Keage et al., 2014). Similarly, another study reported that the prevalence of amyloid positivity on PET in FTLD patients was lower than healthy age-matched controls, further corroborating our findings (Ossenkoppele et al., 2015). Furthermore, reduced amyloid pathology with concomitant exaggerated microglial CD68 levels and activation in TDP-43-positive ALS cases strongly supports our hypothesis (as also observed in Brettschneider et al., 2012).

Emerging evidence suggests that clearance mechanisms play a crucial role in neurodegenerative disorders, particularly in sporadic cases where no mutations may cause the disease. In addition, genome-wide association studies (GWASs) have identified a growing number of risk factors associated with microglial function. Certainly, identifying the pathways that underlie microglia-induced pathological synaptic pruning is of foremost importance. These pathways could elucidate cellular mechanisms common to the early stages of many distinct neurodegenerative disorders and may also reveal new powerful and efficient therapeutic targets. We believe these interventions could selectively target the paradoxical effects we discovered to prevent synapse loss and cognitive decline.

STAR★METHODS

Detailed methods are provided in the online version of this paper and include the following:

- KEY RESOURCES TABLE
- CONTACT FOR REAGENT AND RESOURCE SHARING
- EXPERIMENTAL MODEL AND SUBJECT DETAILS
  - Animal studies
  - Human studies
- METHODS DETAILS
  - Cell Culture
  - siRNAs
  - Acute Isolation of Adult Microglia
  - Aβ Clearance Assay and Cell Proliferation Assay
  - Aβ measurement
  - Phagocytosis and degradation of fluorescently labeled Aβ
  - Western Blot and Brain Tissue protein extracts
  - Stereotactic injections of Aβ
  - Immunohistochemistry and Microscopy
  - Human Sample Processing For Aβ/ TDP-43 detection
  - Human samples Immunofluorescence Protocol
- QUANTIFICATION AND STATISTICAL ANALYSIS

SUPPLEMENTAL INFORMATION

Supplemental Information includes six figures, two tables, and one movie and can be found with this article online at http://dx.doi.org/10.1016/j.neuron.2017.05.037.

AUTHOR CONTRIBUTIONS

R.C.P., M.M., and A.V. performed *in vitro* and animal experiments. A.J., S.A., and P.E.S. designed and conducted the clinical studies. J.L.R., E.B.L., V.M.-Y.L., and J.Q.T. designed and conducted the post-mortem examination relative to the amyloid burden. C.M.H., J.R., and T.S.-J. conducted the post-mortem examination relative to CD68 and pTDP-43-microglia co-localization in ALS cases. R.C.P. and L.R. conceived the project, designed the experiments, and wrote the manuscript. All authors contributed to the edits of the paper.

ACKNOWLEDGMENTS

This work was supported by Swiss National Science Foundation (SNF), Synapsis Foundation Alzheimer Research Switzerland ARS, Velux Stiftung, Cure Alzheimer Fund, Sinergia grant, and Interdisciplinary Core grant of the SNF. R.C.P. was funded by Forschungskredit University of Zurich. T.S.-J. and C.M.H. were funded by Alzheimer's Research UK, European Research Council and MND Scotland. We wish to thank all of our patient donors and their families for their valuable contributions to this work. We greatly acknowledge the work of Prof. Colin Smith and Chris-Anne MacKenzie from the Edinburgh Brain Bank for the provision of human tissue. The Edinburgh Brain Bank is a Medical Research Council funded facility with research ethics committee (REC) approval (11/ES/0022). We are grateful to the MND Register, hosted by the Euan Macdonald Centre for MND Research and funded by MND Scotland. In addition, thanks to Motor Neurone Disease Scotland for supporting the work of C.M.H. T.S.-J is supported by the European Research Council (ALZSYN), Alzheimer's Research UK and the Scottish Government Chief Scientist Office, a Wellcome Trust-University of Edinburgh Institutional Strategic Support Fund, Alzheimer's Society, and would like to acknowledge the FENS Kavli Network of Excellence.

Received: September 12, 2016
Revised: January 28, 2017
Accepted: May 26, 2017
Published: June 29, 2017

REFERENCES

Arnold, S.E., Toledo, J.B., Appleby, D.H., Xie, S.X., Wang, L.S., Baek, Y., Wolk, D.A., Lee, E.B., Miller, B.L., Lee, V.M., and Trojanowski, J.Q. (2013). Comparative survey of the topographical distribution of signature molecular lesions in major neurodegenerative diseases. J. Comp. Neurol. *521*, 4339–4355.

Bali, J., Gheinani, A.H., Zurbriggen, S., and Rajendran, L. (2012). Role of genes linked to sporadic Alzheimer's disease risk in the production of β-amyloid peptides. Proc. Natl. Acad. Sci. USA *109*, 15307–15311.

Baralle, M., Buratti, E., and Baralle, F.E. (2013). The role of TDP-43 in the pathogenesis of ALS and FTLD. Biochem. Soc. Trans. *41*, 1536–1540.

Boluda, S., Toledo, J.B., Irwin, D.J., Raible, K.M., Byrne, M.D., Lee, E.B., Lee, V.M., and Trojanowski, J.Q. (2014). A comparison of Aβ amyloid pathology staging systems and correlation with clinical diagnosis. Acta Neuropathol. *128*, 543–550.

Braak, H., and Braak, E. (1998). Evolution of neuronal changes in the course of Alzheimer's disease. J. Neural Transm. Suppl. *53*, 127–140.

Brettschneider, J., Toledo, J.B., Van Deerlin, V.M., Elman, L., McCluskey, L., Lee, V.M., and Trojanowski, J.Q. (2012). Microglial activation correlates with disease progression and upper motor neuron clinical symptoms in amyotrophic lateral sclerosis. PLoS ONE *7*, e39216.

Brooks, B.R. (1994). El Escorial World Federation of Neurology criteria for the diagnosis of amyotrophic lateral sclerosis. Subcommittee on Motor Neuron Diseases/Amyotrophic Lateral Sclerosis of the World Federation of Neurology Research Group on Neuromuscular Diseases and the El Escorial "Clinical limits of amyotrophic lateral sclerosis" workshop contributors. J. Neurol. Sci. *124* (*Suppl*), 96–107.

Buratti, E., and Baralle, F.E. (2001). Characterization and functional implications of the RNA binding properties of nuclear factor TDP-43, a novel splicing regulator of CFTR exon 9. J. Biol. Chem. *276*, 36337–36343.

Buratti, E., and Baralle, F.E. (2009). The molecular links between TDP-43 dysfunction and neurodegeneration. Adv. Genet. *66*, 1–34.

Chiang, P.M., Ling, J., Jeong, Y.H., Price, D.L., Aja, S.M., and Wong, P.C. (2010). Deletion of TDP-43 down-regulates Tbc1d1, a gene linked to obesity, and alters body fat metabolism. Proc. Natl. Acad. Sci. USA *107*, 16320–16324.

Cohen, T.J., Lee, V.M., and Trojanowski, J.Q. (2011). TDP-43 functions and pathogenic mechanisms implicated in TDP-43 proteinopathies. Trends Mol. Med. *17*, 659–667.

Cole, G.M., Bell, L., Truong, Q.B., and Saitoh, T. (1992). An endosomal-lysosomal pathway for degradation of amyloid precursor protein. Ann. N Y Acad. Sci. *674*, 103–117.

Cook, C., Zhang, Y.J., Xu, Y.F., Dickson, D.W., and Petrucelli, L. (2008). TDP-43 in neurodegenerative disorders. Expert Opin. Biol. Ther. *8*, 969–978.

Davalos, D., Grutzendler, J., Yang, G., Kim, J.V., Zuo, Y., Jung, S., Littman, D.R., Dustin, M.L., and Gan, W.B. (2005). ATP mediates rapid microglial response to local brain injury in vivo. Nat. Neurosci. *8*, 752–758.

Deierborg, T. (2013). Preparation of primary microglia cultures from postnatal mouse and rat brains. Methods Mol. Biol. *1041*, 25–31.

Derecki, N.C., Katzmarski, N., Kipnis, J., and Meyer-Luehmann, M. (2014). Microglia as a critical player in both developmental and late-life CNS pathologies. Acta Neuropathol. *128*, 333–345.

Diaper, D.C., Adachi, Y., Sutcliffe, B., Humphrey, D.M., Elliott, C.J., Stepto, A., Ludlow, Z.N., Vanden Broeck, L., Callaerts, P., Dermaut, B., et al. (2013). Loss and gain of Drosophila TDP-43 impair synaptic efficacy and motor control leading to age-related neurodegeneration by loss-of-function phenotypes. Hum. Mol. Genet. *22*, 1539–1557.

Fa, M., Orozco, I.J., Francis, Y.I., Saeed, F., Gong, Y., and Arancio, O. (2010). Preparation of oligomeric beta-amyloid 1-42 and induction of synaptic plasticity impairment on hippocampal slices. J. Vis. Exp. (41), 1884.

Feng, G., Mellor, R.H., Bernstein, M., Keller-Peck, C., Nguyen, Q.T., Wallace, M., Nerbonne, J.M., Lichtman, J.W., and Sanes, J.R. (2000). Imaging neuronal subsets in transgenic mice expressing multiple spectral variants of GFP. Neuron *28*, 41–51.

Frenkel, D., Wilkinson, K., Zhao, L., Hickman, S.E., Means, T.K., Puckett, L., Farfara, D., Kingery, N.D., Weiner, H.L., and El Khoury, J. (2013). Scara1 deficiency impairs clearance of soluble amyloid-β by mononuclear phagocytes and accelerates Alzheimer's-like disease progression. Nat. Commun. *4*, 2030.

Gendron, T.F., and Petrucelli, L. (2011). Rodent models of TDP-43 proteinopathy: investigating the mechanisms of TDP-43-mediated neurodegeneration. J. Mol. Neurosci. *45*, 486–499.

Goldmann, T., Wieghofer, P., Jordão, M.J., Prutek, F., Hagemeyer, N., Frenzel, K., Amann, L., Staszewski, O., Kierdorf, K., Krueger, M., et al. (2016). Origin, fate and dynamics of macrophages at central nervous system interfaces. Nat. Immunol. *17*, 797–805.

Handley, E.E., Pitman, K.A., Dawkins, E., Young, K.M., Clark, R.M., Jiang, T.C., Turner, B.J., Dickson, T.C., and Blizzard, C.A. (2016). Synapse Dysfunction of Layer V Pyramidal Neurons Precedes Neurodegeneration in a Mouse Model of TDP-43 Proteinopathies. Cereb Cortex. Published online August 5, 2016. http://dx.doi.org/10.1093/cercor/bhw185.

Hebert, L.E., Weuve, J., Scherr, P.A., and Evans, D.A. (2013). Alzheimer disease in the United States (2010-2050) estimated using the 2010 census. Neurology *80*, 1778–1783.

Hong, S., Beja-Glasser, V.F., Nfonoyim, B.M., Frouin, A., Li, S., Ramakrishnan, S., Merry, K.M., Shi, Q., Rosenthal, A., Barres, B.A., et al. (2016). Complement and microglia mediate early synapse loss in Alzheimer mouse models. Science *352*, 712–716.

Igaz, L.M., Kwong, L.K., Lee, E.B., Chen-Plotkin, A., Swanson, E., Unger, T., Malunda, J., Xu, Y., Winton, M.J., Trojanowski, J.Q., and Lee, V.M. (2011). Dysregulation of the ALS-associated gene TDP-43 leads to neuronal death and degeneration in mice. J. Clin. Invest. *121*, 726–738.

Iguchi, Y., Katsuno, M., Niwa, J., Takagi, S., Ishigaki, S., Ikenaka, K., Kawai, K., Watanabe, H., Yamanaka, K., Takahashi, R., et al. (2013). Loss of TDP-43 causes age-dependent progressive motor neuron degeneration. Brain *136*, 1371–1382.

Jawaid, A., Murthy, S.B., Wilson, A.M., Qureshi, S.U., Amro, M.J., Wheaton, M., Simpson, E., Harati, Y., Strutt, A.M., York, M.K., and Schulz, P.E. (2010). A decrease in body mass index is associated with faster progression of motor symptoms and shorter survival in ALS. Amyotroph. Lateral Scler. *11*, 542–548.

Keage, H.A., Hunter, S., Matthews, F.E., Ince, P.G., Hodges, J., Hokkanen, S.R., Highley, J.R., Dening, T., and Brayne, C. (2014). TDP-43 pathology in the population: prevalence and associations with dementia and age. J. Alzheimers Dis. *42*, 641–650.

Kettenmann, H., Kirchhoff, F., and Verkhratsky, A. (2013). Microglia: new roles for the synaptic stripper. Neuron *77*, 10–18.

Knobloch, M., Konietzko, U., Krebs, D.C., and Nitsch, R.M. (2007). Intracellular Abeta and cognitive deficits precede beta-amyloid deposition in transgenic arcAbeta mice. Neurobiol. Aging *28*, 1297–1306.

Kraemer, B.C., Schuck, T., Wheeler, J.M., Robinson, L.C., Trojanowski, J.Q., Lee, V.M., and Schellenberg, G.D. (2010). Loss of murine TDP-43 disrupts motor function and plays an essential role in embryogenesis. Acta Neuropathol. *119*, 409–419.

LaClair, K.D., Donde, A., Ling, J.P., Jeong, Y.H., Chhabra, R., Martin, L.J., and Wong, P.C. (2016). Depletion of TDP-43 decreases fibril and plaque β-amyloid and exacerbates neurodegeneration in an Alzheimer's mouse model. Acta Neuropathol. *132*, 859–873.

Lagier-Tourenne, C., Polymenidou, M., and Cleveland, D.W. (2010). TDP-43 and FUS/TLS: emerging roles in RNA processing and neurodegeneration. Hum. Mol. Genet. *19* (R1), R46–R64.

Lee, C.Y., and Landreth, G.E. (2010). The role of microglia in amyloid clearance from the AD brain. J. Neural Transm. (Vienna) *117*, 949–960.

Lee, E.B., Leng, L.Z., Zhang, B., Kwong, L., Trojanowski, J.Q., Abel, T., and Lee, V.M. (2006). Targeting amyloid-beta peptide (Abeta) oligomers by passive immunization with a conformation-selective monoclonal antibody improves learning and memory in Abeta precursor protein (APP) transgenic mice. J. Biol. Chem. *281*, 4292–4299.

McKhann, G., Drachman, D., Folstein, M., Katzman, R., Price, D., and Stadlan, E.M. (1984). Clinical diagnosis of Alzheimer's disease: report of the NINCDS-ADRDA Work Group under the auspices of Department of Health and Human Services Task Force on Alzheimer's Disease. Neurology *34*, 939–944.

Medina, D.X., Orr, M.E., and Oddo, S. (2014). Accumulation of C-terminal fragments of transactive response DNA-binding protein 43 leads to synaptic loss and cognitive deficits in human TDP-43 transgenic mice. Neurobiol. Aging *35*, 79–87.

Nakanishi, H. (2003). Microglial functions and proteases. Mol. Neurobiol. *27*, 163–176.

Neary, D., Snowden, J.S., Gustafson, L., Passant, U., Stuss, D., Black, S., Freedman, M., Kertesz, A., Robert, P.H., Albert, M., et al. (1998). Frontotemporal

lobar degeneration: a consensus on clinical diagnostic criteria. Neurology *51*, 1546–1554.

Nelson, P.T., Alafuzoff, I., Bigio, E.H., Bouras, C., Braak, H., Cairns, N.J., Castellani, R.J., Crain, B.J., Davies, P., Del Tredici, K., et al. (2012). Correlation of Alzheimer disease neuropathologic changes with cognitive status: a review of the literature. J. Neuropathol. Exp. Neurol. *71*, 362–381.

Neumann, M., Sampathu, D.M., Kwong, L.K., Truax, A.C., Micsenyi, M.C., Chou, T.T., Bruce, J., Schuck, T., Grossman, M., Clark, C.M., et al. (2006). Ubiquitinated TDP-43 in frontotemporal lobar degeneration and amyotrophic lateral sclerosis. Science *314*, 130–133.

Neumann, M., Kwong, L.K., Lee, E.B., Kremmer, E., Flatley, A., Xu, Y., Forman, M.S., Troost, D., Kretzschmar, H.A., Trojanowski, J.Q., and Lee, V.M. (2009). Phosphorylation of S409/410 of TDP-43 is a consistent feature in all sporadic and familial forms of TDP-43 proteinopathies. Acta Neuropathol. *117*, 137–149.

Nimmerjahn, A., Kirchhoff, F., and Helmchen, F. (2005). Resting microglial cells are highly dynamic surveillants of brain parenchyma in vivo. Science *308*, 1314–1318.

Ossenkoppele, R., Jansen, W.J., Rabinovici, G.D., Knol, D.L., van der Flier, W.M., van Berckel, B.N., Scheltens, P., Visser, P.J., Verfaillie, S.C., Zwan, M.D., et al.; Amyloid PET Study Group (2015). Prevalence of amyloid PET positivity in dementia syndromes: a meta-analysis. JAMA *313*, 1939–1949.

Paolicelli, R.C., and Gross, C.T. (2011). Microglia in development: linking brain wiring to brain environment. Neuron Glia Biol. *7*, 77–83.

Paolicelli, R.C., Bolasco, G., Pagani, F., Maggi, L., Scianni, M., Panzanelli, P., Giustetto, M., Ferreira, T.A., Guiducci, E., Dumas, L., et al. (2011). Synaptic pruning by microglia is necessary for normal brain development. Science *333*, 1456–1458.

Paresce, D.M., Ghosh, R.N., and Maxfield, F.R. (1996). Microglial cells internalize aggregates of the Alzheimer's disease amyloid beta-protein via a scavenger receptor. Neuron *17*, 553–565.

Parkhurst, C.N., Yang, G., Ninan, I., Savas, J.N., Yates, J.R., 3rd, Lafaille, J.J., Hempstead, B.L., Littman, D.R., and Gan, W.B. (2013). Microglia promote learning-dependent synapse formation through brain-derived neurotrophic factor. Cell *155*, 1596–1609.

Polymenidou, M., Lagier-Tourenne, C., Hutt, K.R., Huelga, S.C., Moran, J., Liang, T.Y., Ling, S.C., Sun, E., Wancewicz, E., Mazur, C., et al. (2011). Long pre-mRNA depletion and RNA missplicing contribute to neuronal vulnerability from loss of TDP-43. Nat. Neurosci. *14*, 459–468.

Prinz, M., Priller, J., Sisodia, S.S., and Ransohoff, R.M. (2011). Heterogeneity of CNS myeloid cells and their roles in neurodegeneration. Nat. Neurosci. *14*, 1227–1235.

Ries, M., and Sastre, M. (2016). Mechanisms of Aβ Clearance and Degradation by Glial Cells. Front. Aging Neurosci. *8*, 160.

Romano, G., Appocher, C., Scorzeto, M., Klima, R., Baralle, F.E., Megighian, A., and Feiguin, F. (2015). Glial TDP-43 regulates axon wrapping, GluRIIA clustering and fly motility by autonomous and non-autonomous mechanisms. Hum. Mol. Genet. *24*, 6134–6145.

Schafer, D.P., Lehrman, E.K., Kautzman, A.G., Koyama, R., Mardinly, A.R., Yamasaki, R., Ransohoff, R.M., Greenberg, M.E., Barres, B.A., and Stevens, B. (2012). Microglia sculpt postnatal neural circuits in an activity and complement-dependent manner. Neuron *74*, 691–705.

Serrano-Pozo, A., Frosch, M.P., Masliah, E., and Hyman, B.T. (2011). Neuropathological alterations in Alzheimer disease. Cold Spring Harb. Perspect. Med. *1*, a006189.

Sierra, A., Encinas, J.M., Deudero, J.J., Chancey, J.H., Enikolopov, G., Overstreet-Wadiche, L.S., Tsirka, S.E., and Maletic-Savatic, M. (2010). Microglia shape adult hippocampal neurogenesis through apoptosis-coupled phagocytosis. Cell Stem Cell *7*, 483–495.

Solé-Domènech, S., Cruz, D.L., Capetillo-Zarate, E., and Maxfield, F.R. (2016). The endocytic pathway in microglia during health, aging and Alzheimer's disease. Ageing Res. Rev. *32*, 89–103.

Terry, R.D., Masliah, E., Salmon, D.P., Butters, N., DeTeresa, R., Hill, R., Hansen, L.A., and Katzman, R. (1991). Physical basis of cognitive alterations in Alzheimer's disease: synapse loss is the major correlate of cognitive impairment. Ann. Neurol. *30*, 572–580.

Toledo, J.B., Van Deerlin, V.M., Lee, E.B., Suh, E., Baek, Y., Robinson, J.L., Xie, S.X., McBride, J., Wood, E.M., Schuck, T., et al. (2014). A platform for discovery: The University of Pennsylvania Integrated Neurodegenerative Disease Biobank. Alzheimers Dement. *10*, 477–484.

Tremblay, M.E., Stevens, B., Sierra, A., Wake, H., Bessis, A., and Nimmerjahn, A. (2011). The role of microglia in the healthy brain. J. Neurosci. *31*, 16064–16069.

Vanden Broeck, L., Naval-Sánchez, M., Adachi, Y., Diaper, D., Dourlen, P., Chapuis, J., Kleinberger, G., Gistelinck, M., Van Broeckhoven, C., Lambert, J.C., et al. (2013). TDP-43 loss-of-function causes neuronal loss due to defective steroid receptor-mediated gene program switching in Drosophila. Cell Rep. *3*, 160–172.

Vekrellis, K., Ye, Z., Qiu, W.Q., Walsh, D., Hartley, D., Chesneau, V., Rosner, M.R., and Selkoe, D.J. (2000). Neurons regulate extracellular levels of amyloid beta-protein via proteolysis by insulin-degrading enzyme. J. Neurosci. *20*, 1657–1665.

Wakselman, S., Béchade, C., Roumier, A., Bernard, D., Triller, A., and Bessis, A. (2008). Developmental neuronal death in hippocampus requires the microglial CD11b integrin and DAP12 immunoreceptor. J. Neurosci. *28*, 8138–8143.

Walker, A.K., Tripathy, K., Restrepo, C.R., Ge, G., Xu, Y., Kwong, L.K., Trojanowski, J.Q., and Lee, V.M. (2015). An insoluble frontotemporal lobar degeneration-associated TDP-43 C-terminal fragment causes neurodegeneration and hippocampus pathology in transgenic mice. Hum. Mol. Genet. *24*, 7241–7254.

Wu, L.S., Cheng, W.C., and Shen, C.K. (2012). Targeted depletion of TDP-43 expression in the spinal cord motor neurons leads to the development of amyotrophic lateral sclerosis-like phenotypes in mice. J. Biol. Chem. *287*, 27335–27344.

Xia, Q., Wang, H., Hao, Z., Fu, C., Hu, Q., Gao, F., Ren, H., Chen, D., Han, J., Ying, Z., and Wang, G. (2016). TDP-43 loss of function increases TFEB activity and blocks autophagosome-lysosome fusion. EMBO J. *35*, 121–142.

Xu, Y.F., Zhang, Y.J., Lin, W.L., Cao, X., Stetler, C., Dickson, D.W., Lewis, J., and Petrucelli, L. (2011). Expression of mutant TDP-43 induces neuronal dysfunction in transgenic mice. Mol. Neurodegener. *6*, 73.

Yang, C., Wang, H., Qiao, T., Yang, B., Aliaga, L., Qiu, L., Tan, W., Salameh, J., McKenna-Yasek, D.M., Smith, T., et al. (2014). Partial loss of TDP-43 function causes phenotypes of amyotrophic lateral sclerosis. Proc. Natl. Acad. Sci. USA *111*, E1121–E1129.

Ying, Z., Xia, Q., Hao, Z., Xu, D., Wang, M., Wang, H., and Wang, G. (2016). TARDBP/TDP-43 regulates autophagy in both MTORC1-dependent and MTORC1-independent manners. Autophagy *12*, 707–708.

STAR★METHODS

KEY RESOURCES TABLE

REAGENT or RESOURCE	SOURCE	IDENTIFIER
Antibodies		
Rabbit polyclonal anti-TDP-43	Proteintech	Cat. 0782-2-AP; RRID: AB_615042
Rat monoclonal anti-LAMP-1	DSHB	Cat. 1D4B; RRID: AB_2134500
Rat monoclonal anti-LAMP-2	DSHB	Cat. ABL-93, RRID: AB_2134767
Mouse monoclonal anti-PSD-95 clone 6G6-1C9	Millipore	Cat. MAB1596, RRID: AB_2092365
Mouse monoclonal anti-VGLUT1	Synaptic System	Cat. 135511
Rabbit polyclonal anti-Synapsin I	Thermo Fisher Scientific	Cat. A-6442, RRID: AB_2536207
Rabbit monoclonal anti-Synaptophysin	Abcam	Cat. ab52636
Rat monoclonal anti-Myelin Basic Protein	Abcam	Cat. ab7349, RRID: AB_305869
Mouse monoclonal anti-MAP2	Abcam	Cat. ab11267, RRID: AB_297885
Mouse monoclonal anti-GAPDH	Ambion	Cat. AM4300, RRID: AB_437392
Mouse monoclonal anti-beta actin	Abcam	Cat. ab8226, RRID: AB_306371
Rabbit polyclonal anti-Iba1	Wako	Cat. 27030, RRID: AB_2314667
Mouse monoclonal anti-beta amyloid 1-16	BioLegend	Cat# 803013, RRID: AB_2564765
Rat monoclonal anti-CD68	Bio-Rad / AbD Serotec	Cat. MCA1957, RRID: AB_322219)
Rat monoclonal anti-TDP43 Phospho (Ser409/410)	Gift of Dr. Manuela Neumann	1D3
Mouse monoclonal anti-beta amyloid	CNDR	Cat# NAB228, RRID: AB_2314850
Mouse monoclonal anti-CD68	Dako	Cat. M0876, RRID: AB_2074844)
Biological Samples		
Human post-mortem samples	Centre for Neurodegenerative Disease Research (CNDR), Pennsylvania, USA	N/A
Human post-mortem samples	Edinburgh Brain Bank	N/A
Chemicals, Peptides, and Recombinant Proteins		
Tamoxifen	Sigma-Aldrich	T5648; CAS: 10540-29-1
LysoTracker Red DND-99	Invitrogen/Molecular Probes	Cat. No. L7528
Lipofectamine2000	Invitrogen	Cat. 11668027
TAT-CRE Recombinase	Millipore	Cat. SCR508
Beta - Amyloid (1 - 40), HiLyte Fluor 647	Anaspec	Cat. AS-60493
Beta - Amyloid (1 - 40), TAMRA labeled	Anaspec	Cat. AS-60488
Beta - Amyloid (1 - 42), Human	Anaspec	Cat. AS-20276
Dextran, Alexa Fluor 647	Molecular Probes	Cat. D22914
Transferrin, Alexa Fluor 555, 568	Molecular Probes	Cat. T35352,T23365
Thioflavin S	Sigma-Aldrich	Cat. T1892, Cas no. 1326-12-1
Critical Commercial Assays		
Multi-Array Multiplex Kit for Aβ40, Aβ42 and sAPPβ	Meso Scale Discovery	Cat. N31CB-1, Cat. K15200E
Experimental Models: Cell Lines		
Mouse: BV-2	Prof. Frei, UZH	RRID: CVCL_0182
Human: HeLa swAPP	Prof. Yu, Dallas, USA	N/A
Mouse: Primary microglia from Tardbptm1.1Pcw/J	The Jackson Laboratory	Stock No: 017591
Experimental Models: Organisms/Strains		
Mouse: Cx3cr1tm2.1(cre/ERT2)Litt/WganJ	The Jackson Laboratory	Stock No: 021160
Mouse: Tardbptm1.1Pcw/J	The Jackson Laboratory	Stock No: 017591

(*Continued on next page*)

Continued		
REAGENT or RESOURCE	SOURCE	IDENTIFIER
Mouse: Tg(Thy1-EGFP)MJrs/J	The Jackson Laboratory	Stock No: 007788
Mouse: Tg ArcAβ (hAPP Arc/Swe)	University of Zurich	N/A; Knobloch et al., 2007
Oligonucleotides		
Tardbp Stealth RNAi Oligo: CGAAAGGGUUUGGCUUUGUUCGAUU	Invitrogen	Cat. 1320001 230908-MSS214148
Tardbp Stealth RNAi Oligo: GCAAUCUGGUAUAUGUUGUCAACUA	Invitrogen	Cat. 1320001 230908-MSS214149
Tardbp Stealth RNAi Oligo: GAAAUACCAUCAGAAGACGAUGGGA	Invitrogen	Cat. 1320001 230908-MSS214150
Tardbp Stealth RNAi Oligo: AGGAAUACUUCUGUCUACAUGCUUU	Invitrogen	Cat. N/A 230908-MSS-seq
Software and Algorithms		
Imaris Software	Bitplane	http://www.bitplane.com/
ImageJ Software	NIH	https://imagej.nih.gov/ij/
Prism 7	GraphPad	http://www.graphpad.com/scientific-software/prism/

CONTACT FOR REAGENT AND RESOURCE SHARING

Further information and requests for resources and reagents should be directed to and will be fulfilled by the Lead Contact, Prof. Lawrence Rajendran (lawrence.rajendran@irem.uzh.ch).

EXPERIMENTAL MODEL AND SUBJECT DETAILS

Animal studies

Cx3cr1tm2.1(cre/ERT2)Litt/WganJ and Tardbp$^{floxed/floxed}$ mice, originally obtained from Jackson Labs, were maintained on a C57BL/6J genetic background, and were intercrossed to produce the microglia-specific TDP-43 inducible conditional KO mouse line, cKO (Parkhurst et al., 2013; Chiang et al., 2010). APParc (ArcAβ transgenic) mice were produced in our department and maintained in our breeding colony on a C57BL/6J genetic background, and were crossed to the cKO mouse line for studies in a mouse model of AD (Knobloch et al., 2007). All the experimental subjects were obtained by crossing Cx3cr1creERT2/creERT2;Tardbp^{floxed}/^{wt} with Tardbp$^{floxed/wt}$, in order to produce littermates that were all heterozygous for Cx3cr1creERT2, and wild-type (WT) or homozygous (cKO) for the Tardbp^{floxed} allele. Both males and females were used for the experiments, and cKO and WT controls were always paired littermates, sex and age-matched. Importantly, all subjects underwent tamoxifen administration, to rule out any unspecific effect due to the treatment. Tamoxifen (Sigma-Aldrich, Buchs, Switzerland) was dissolved in corn oil (Sigma-Aldrich) and administered via i.p. injections (2 mg/mouse/day for 5 consecutive days) when mice were 4 months old. To reduce bias in the study design, all the experimental subjects were caged in groups and all underwent tamoxifen injections, to equally expose them to the effect of the treatment. For spine density analysis, cKO mice were intercrossed to Thy1-EGFP-M mouse line (Feng et al., 2000). Mice were given *ad libitum* access to food and water and were maintained group housed on a 12:12h light-dark cycle. For stereotactic injection experiments, mice were sacrificed at 5 months. For all the other experiments, mice were sacrificed when they were 7 (APParc; cKO) or 8 months old (cKO). All animal procedures were conducted with approval of the animal care and use committees of the Swiss Cantonal Veterinary Office.

Human studies

Clinical study

The study population was derived from 1818 consecutive ALS patients seen at the Baylor College of Medicine, Houston, TX, USA Neurology outpatient clinic between 1999 to 2008. All patients had diagnosis of clinically probable or possible ALS according to the revised El Escorial criteria (Brooks, 1994). Patients under the age of 65 (n = 273), lacking neuropsychological assessment/AD screening (n = 794), or with over-lapping FTD (n = 41), were excluded. Further exclusions (n = 12) were for patients with a history of neurological conditions potentially impacting cognition, such as stroke, vitamin B12 deficiency, and severe traumatic brain injury. In total, n = 698 patients were included in the study (aged 65-74 n = 530: ALS with AD n = 25, 48% male; ALS without AD n = 505, 59.8% male. Aged $\geq$ 75 n = 168: ALS with AD n = 12, 83.3% male; ALS without AD n = 156, 48.7%, see details in Table S1). All the selected patients had undergone comprehensive neurological and neuropsychological exams by physicians blinded to the current study design at the time of assessment. The neuropsychological battery comprised tests for verbal and non-verbal memory,

executive functioning, semantic fluency, and visuo-spatial functioning as previously described (Jawaid et al., 2010). Patients were labeled with AD or FTD if their clinical and neuropsychological parameters corresponded to the National Institute of Non-communicable Disorders and Stroke- Alzheimer Disease and Related Disorders Association (NINDS-ADRDA) criteria for probable or possible AD (McKhann et al., 1984) or Neary's criteria for FTD (Neary et al., 1998) respectively. Further details are reported in Table S1. Informed written consent was obtained from all the patients. The study was approved by the Institutional review board (IRB) of Baylor College of Medicine, Houston, TX, USA.

Human post-mortem study for amyloid detection

The autopsy cohort comprised, n = 35 ALS patients with clinical diagnosis of ALS in accordance with the modified El escorial criteria with pathological confirmation of TDP-43 pathology, n = 25 FTLD patients with clinical diagnosis of FTD in accordance with the Neary criteria with pathological confirmation of TDP-43 pathology, n = 40 controls who died of non-neurological causes and were negative for TDP-43 pathology, n = 62 patients with clinically probable AD according to NINDS criteria with pathological confirmation of AD on autopsy. The neuropathological diagnoses were established and documented at the Centre for Neurodegenerative Disease Research (CNDR) at the University of Pennsylvania, USA. Informed written consent was obtained from all the patients or their next of kin at the time of death. The autopsies were performed over the course of 22 years (1993-2015) and pathological findings, as well as, clinically relevant information (gender, age of onset, site of onset, age at death, disease severity, etc.) were documented in an integrated database described previously (Toledo et al., 2014).

Human post-mortem study for CD68 and pTDP-43-Iba1 detection

The autopsy cohort comprised n = 11 ALS cases TDP-43-negative (average age 66.8 ± 13.13; mean ± SD), n = 16 ALS cases TDP-43 positive (61.6 ± 10.2), and n = 6 healthy control (78.5 ± 0.8) who died of non-neurological causes and were negative for TDP-43 pathology (for details, see Table S2. Informed written consent was obtained from all the patients or their next of kin at the time of death. Use of human tissue for CD68 post-mortem studies has been reviewed and approved by the Edinburgh Brain Bank ethics committee and the ACCORD medical research ethics committee, AMREC (ACCORD is the Academic and Clinical Central Office for Research and Development, a joint office of the University of Edinburgh and NHS Lothian). The Edinburgh Brain Bank is a Medical Research Council funded facility with research ethics committee (REC) approval (11/ES/0022).

METHODS DETAILS

Cell Culture

BV2 cells and HeLa cells expressing the APP Swedish mutation (HeLa swAPP) were cultured in DMEM (Invitrogen, CA, USA), supplemented with 10% FCS and 100 U mL-1 penicillin/streptomycin, at 37°C and 5% CO2 in a humidified incubator. In addition, HeLa swAPP were supplemented with 0.1% G418 antibiotic (Carl Roth), and 0.1% Zeocin (Invitrogen). Primary microglial murine cell cultures were prepared as described in Deierborg (2013). Briefly, mixed glia cultures were prepared from newborn $Tardbp^{floxed/floxed}$ mice and cultured in high glucose (4.5 mg/ml) DMEM + GlutaMax supplemented with 10% FCS and 100 U mL-1 penicillin/streptomycin. Microglial cells were harvested by manual shake-off after 10-14 days of primary cultivation. The medium containing detached microglia was collected and isolated microglia were reseeded on 96-well plates at a density of 4 × 104 cells/well at 37°C and 5% CO2. Cells were allowed to settle for 24 hr before treatment. Tardbp gene deletion was induced in $Tardbp^{floxed/floxed}$ primary microglia culture by recombinant TAT-CRE treatment (100 U/ml medium, EMD Millipore). Control $Tardbp^{floxed/floxed}$ cells were treated with a solution containing 50% glycerol, 500 mM NaCl and 20 mM HEPES at pH 7.4.

Cells for immunohistochemistry were seeded onto glass coverslips in 96-well plates. Labeling of acidic organelles in BV2 and primary microglia was performed by incubating living cells, at 37°C and 5% CO2, for 90 min with 200 nM LysoTracker Red DND-99 fluorescent dye (Invitrogen).

siRNAs

All siRNAs were chemically synthesized as stealth RNAi from Invitrogen. A pool of four different siRNA per gene (1 scrambled control plus 18 risk genes associated with neurodegenerative disorders) were transfected into BV2 murine cells, for the initial screen. Validation of Tardbp knockdown was performed by using pool or single stealth siRNA oligos. Transfection complexes in technical triplicates were prepared in Opti-mem serum-free medium (Invitrogen) by mixing Lipofectamine 2000 (Invitrogen) and siRNAs (50 nM). BV2 cells were seeded at density of 2,500 cells per well, 24 hr prior the transfection, on 96-well plates coated with poly-D-lysin (Sigma-Aldrich).

Acute Isolation of Adult Microglia

Microglia from the brain of adult mice were acutely isolated according to slight modification of Cardona et al., 2006. Briefly, mice were anaesthetized and perfused with saline solution. Brains were harvested and freed of meninges, then finely minced by scissors in digestion cocktail containing 0.4 mg/ml CollagenaseD (Roche, Rotkreuz, Switzerland) and 0.025U/ml DNaseI (Sigma) in HBSS. The cell suspension was incubated for 45 min on shaking, at 37°C, then filtered through 70μm nylon mesh and washed in HBSS. The pellet was resuspended in 37% isotonic Percoll (Sigma-Aldrich), then underlayed with 70% and overlayed with 30% isotonic Percoll solution. The gradient was spun at 600 g for 30 min at 18°C and afterward the microglia were collected from the 70%–37% interface, washed in HBSS and further processed for RNA isolation.

RT-PCR was used to confirm efficient deletion of Tardbp from primary culture, acutely isolated microglia and whole mouse cortex, and to assess the expression of TFEB-downstream genes in BV2 cells. Total RNA was isolated using Trizol (Invitrogen) according to the manufacturer's protocol. RNA quality and concentration were assessed by a NanoDrop device (Thermo Fisher). Reverse transcription was performed by iScript cDNA synthesis kit (BioRad), according to the manufacturer's recommended instructions. RT-PCR was performed on QuantStudio 7 Flex Real-Time PCR system (Applied Biosystems), by using iQ SYBR Green Supermix (Bio-Rad). Expression levels were compared using the ΔΔCt method normalized to Gapdh.

Aβ Clearance Assay and Cell Proliferation Assay

48 hr after siRNA transfection, BV2 microglia cells were incubated with murine primary neurons- or HeLa swAPP-conditioned medium, and kept overnight at 37°C, 5% CO2. Medium was then collected upon 15 hr of incubation with cells, and used for measurement of residual Aβ. Cell viability was subsequently analyzed with Alamar Blue cell proliferation assay (AbD Serotec) using a fluorescent plate reader (Tecan).

Aβ measurement

96-well and 384-well MULTI-ARRAY Multiplex Kits (Meso Scale Discovery, Gaithersburg, MD, USA) were used to measure the level of Aβ38, Aβ40, Aβ42 and sAPPβ, by electrochemiluminescence (ECL) assay. Supernatants of BV2 cells after the Aβ clearance assay or brain homogenates TBS- and SDS-soluble fractions were further processed according to the manufacturer's instructions. sAPPβ and Aβ species peptides were detected with a monoclonal antibody and quantified by using a SECTOR Imager 6000 reader (Meso Scale Discovery). Values were normalized to scrambled control or to WT, for *in vitro* and *in vivo* experiments, respectively.

Phagocytosis and degradation of fluorescently labeled Aβ

Microglial phagocytosis of fluorescently labeled amyloid (1μM, 647-Aβ40, Anaspec), Dextran (1 mg/ml, Thermo Fisher) and Transferrin (30 μg/ml, Thermo Fisher) was quantified by confocal microscopy after incubation of BV2 cells at 37°C. At the indicated time points, the Aβ-containing medium was removed and cells were washed, fixed with PFA 4%, and incubated with DAPI (Thermo Fisher) for staining the nuclei. For the degradation assay, BV2 cells were incubated for 1 hr with 1 μM TAMRA-Aβ40; after medium removal, cells were washed twice and were either immediately fixed with PFA 4% (T0), either fixed after 3 hr (T3h).

Western Blot and Brain Tissue protein extracts

Cells were lysed in lysis buffer (1% Nonidet P-40 and 0.1% SDS) and brain tissues were homogenized in RIPA buffer (10 mM Tris-Cl pH 8.0, 1 mM EDTA, 150 mM NaCl, 0.5 mM EGTA, 1% Triton X-100, 0.1% sodium deoxycholate), both supplemented with protease inhibitor cocktail (cOmplete, Roche). Protein concentration was determined by BCA assay kit (Thermo Fisher). Cell lysates and brain homogenates were separated on protean TGX precast gels (Biorad) and blotted onto nitrocellulose membranes (Biorad). Membranes were blocked for 60 min with 3% BSA and incubated overnight at 4°C with anti-TDP-43 (1:1000, Proteintech), anti-Rab7 (1:1000, Abcam), anti-LAMP1 (1:1000, DSHB), LAMP2 (1:1000, DSHB, Iowa, USA), anti-PSD95 (1:1000, Millipore), anti-vGlut1 (1:1000, Synaptic Systems), anti-Synapsin (1:1000, Abcam), anti-Synaptophysin (1:1000, Abcam), anti-MBP (1:1000, Abcam), anti-MAP2 (1:1000, Abcam). Protein load was normalized detecting GAPDH (1:5000, Ambion) and β-actin (1:5000, Abcam). After washing membranes were incubated for 60 min with IRDye fluorescent secondary antibody (Li-Cor, Rockland). For detection of Aβ in mouse brain, tissues were processed as follows: homogenization was performed using a glass Teflon homogenizer in 5-fold wet weight amount of TBS solution (50 mM Tris–Cl pH 7.5, 150 mM NaCl) supplemented with protease inhibitor cocktail (cOmplete, Roche). Supernatants were collected (TBS-soluble fraction) after centrifugation at 100,000 g for 1 hr. The pellets were re-homogenized in TBS-protease inhibitor cocktail containing 2% sodium dodecyl sulfate (SDS). Centrifugation was repeated and supernatants were collected (SDS-soluble fraction) and stored at −80°C for further analysis.

Stereotactic injections of Aβ

Aβ42 oligomers were prepared as in Fa et al. (2010). Briefly, human Aβ42 peptide (Anaspec) was dissolved in HFIP, dried overnight RT, then resuspended in DMSO at 5 mM. On the day prior experiment, Aβ was diluted to 100 μM in ACSF and incubated for 12 hr overnight at 4°C, allowing oligomers formation. Just before use, Aβ42 oligomers were spun down at 14000 g for 10 min, mice were anesthetized and 4.5 μL were injected per mouse (0.15 μL/min) according to the following stereotactic coordinates: 0.5 mm posterior to bregma, 1.6 mm lateral to the midline, 1.4 mm ventral. After 24 hr, mice were transcardiacally perfused with 4% PFA, brains were harvested, post-fixed overnight and further processed for immunohistochemistry.

Immunohistochemistry and Microscopy

BV2 cells and primary microglia were fixed in PFA 4%, permeabilized for 5min at room temperature (RT) in 0.25% Triton X-100 and blocked in 2% BSA 0.25% Triton X-100 for 1 hr. Primary antibody incubation was performed overnight in blocking solution at 4°C (Iba1 1:600, Wako Chemicals, Japan; LAMP-2 1:200, TDP-43 1:200, Proteintech Group, IL, USA). Mice were anesthetized with ketamine/xylazine and transcardially perfused with ice cold HBSS (Invitrogen). Brains were harvested and the hemibrains dissected. Right hemispheres, kept for histological investigations, were post-fixed overnight in PFA 4%. Serial coronal sections were cut on a vibratome (60 μm, Leica Microsystems). The left hemibrain was dissected and frozen immediately at −80°C for biochemical

analyses. For antibody staining, brain sections were permeabilized at room temperature (RT) in 0.5% Triton X-100 (Sigma), followed by 1 hr RT blocking in 2% BSA 0.5% Triton X-100 and overnight incubation with primary antibody (Iba1 1:600, Wako Chemicals, Japan; 6E10 1:100, Biolegend; vGlut1 1:100, Synaptic Systems; CD68 1:400, Serotec; PSD-95 1:100, Millipore) at 4°C. Upon washing, sections were incubated 2 hr RT with Alexa-fluorophore-conjugated secondary antibodies (Invitrogen).

For detection of plaques (β sheets positive structures), brain sections were previously incubated with 1% Thioflavin S (ThioS, Sigma, St. Louis, Missouri USA) in 50% EtOH for 5 min, washed twice with 50% ethanol, followed by water and PBS washes, and then subjected to antibody staining as described above.

For spine density, confocal stacks were acquired from the motor/ somatosensory cortex of Thy1-EGFP;Tardbp WT or cKO littermates, based on the GFP signal, and no further staining was required.

Confocal microscopy was performed with a TCS-SP8 (Leica) Laser Scanning System and images were processed and analyzed by ImageJ Software or Imaris Software (Bitplane, Switzerland), as appropriate. Imaris was used for 3D rendering of confocal images for colocalization of volumes and quantification analysis.

Human Sample Processing For Aβ/ TDP-43 detection

Brain extraction, tissue processing, and histological assessments were performed as previously described (Arnold et al., 2013). Briefly, after weighing and gross examination, the cerebral cortices were separated into 1-2 cm sections for further evaluation. Tissue from different brain areas was treated with 10% formalin, paraffin-embedded, cut into 6 μM sections, and stained with hematoxylin-eosin. Immunohistochemistry was performed using anti-bodies against Aβ and phosphorylated TDP-43 (Arnold et al., 2013). Antibody used for Aβ was NAB228, a monoclonal antibody against Aβ applied at a dilution of 1:15000 (Lee et al., 2006). Phosphorylated TDP-43 was stained with a rat monoclonal corresponding to the amino acid residues 404-413 of human TDP-43 and phosphoserine 409/410 (Neumann et al., 2009).

For CD68 detection: Fresh post-mortem tissue blocks (approximately 1 cm3) were fixed in 10% formalin for a minimum of 24 hr. Tissue was dehydrated in an ascending series of alcohol (70%–100%), followed by three xylene washes, all for 4 hr each. Next, three paraffin waxing stages (5 hr each) were performed to ensure full penetration of the embedding wax and then allowed to cool. Sections were cut on a Leica microtome at 4 μm and collected on glass slides. Sections were dried at 40°C for at least 24 hr before staining. Immunohistochemistry was performed using standard protocols following a 3min citric acid pretreatment step in a pressure cooker, enhanced using the Novolink Polymer detection system and visualized using 3,3′-Diaminobenzidine (DAB) as chromogen. CD68 primary antibody (Dako, M0876) was used at 1:100 dilution. Slides were finally counterstained with hematoxylin for 30 s to stain cell nuclei.

Human samples Immunofluorescence Protocol

Formalin-fixed paraffin-embedded (FFPE) slides were de-waxed using standard protocols and treated with picric acid for 15 min. Slides were washed until clear and then placed in 5% Citric Acid (pH 6.0) and pressure cooked to 125oC for 30 s before allowing to cool. Slides were then coated in autofluorescence eliminator (Merck, Millipore) for 5 min before washing twice in PBS. Blocking solution (5% BSA/TBS/0.2% Triton X) was applied for 1 hr before primary antibodies (Rabbit α Iba1 – WAKO, WDR2342 (1:750); Mouse α pTDP43 (s409/s410) – Cosmo Bio Co, TIP-PTD-M01 (1:4000) were added overnight at 4oC in blocking solution. Slides were washed the next day 3 times with TBS + 0.2% Triton for 5 min each, before adding secondary antibodies (Alexa Fluor 546 Goat αMouse IgG – Molecular Probes, A11003 (1:500); Alexa Fluor 488 Goat αRabbit IgG – Life Technologies, A11008 (1:500) and DAPI for 2 hr at RT. Slides were coverslipped with standard mounting media and allowed to dry overnight at room temperature. Images were captured using a Zeiss AxioScan Slide Scanner Z.1 at 20x and at 63x with a Zeiss LSM510 Confocal microscope.

QUANTIFICATION AND STATISTICAL ANALYSIS

For Aβ clearance quantification, the residual Aβ levels measured upon incubation with BV2 cells or primary microglia (see Method Details) were normalized to the scrambled control and then multiplied for the viability index (Alamar Blue absolute counts, normalized to the scrambled control). Technical triplicates were averaged, in three different biological experiments. For quantification of fluorescently labeled cargos, the specific signal internalized by each cell was measured as percentage of area covered per cell, by using ImageJ Software. For western blot analysis, immunoreactivity was detected and quantified by using the Odyssey infrared Imaging System (Li-Cor), and normalized to reference genes, β-actin and GAPDH.

3D imaging analysis was performed by applying recorded algorithms (fixed thresholds for signal intensity and voxel) to all the images of the same experiment, in order to produce unbiased signal quantification. PSD-95 engulfment analysis was performed by quantifying the PSD-95 positive volume present in the Iba1 channel (using the mask function). The engulfed PSD-95 volume was then normalized to the Iba1 and to the total PSD-95 volume in the same acquisition frame.

Spine density analysis was manually conducted by the experimenter and performed blind to genotype. The number of spines per 10 μm was quantified in the cortical layers II/III of cKO;Thy1-GFP mice, on secondary and tertiary apical dendrites.

For quantification of Aβ and TDP-43 in human samples: sixteen different brain regions in limbic cortices, isocortical association areas, sub-cortical regions, and brain stem were assessed for grading of Aβ and TDP-43 pathology. The global burden of pathological lesions was semiquantitatively graded on a four-point scale in each of the sixteen regions by experienced neuropathologists

and neuropathology fellows blinded to the current study design at the time of evaluation (0 = none, 1 = rare/mild, 2 = occasional/moderate, 3 = numerous/severe).

For CD68 quantification in human samples, all sections were assessed using Stereo Investigator. Cortical gray matter was outlined in each section and immune-positive objects identified using an automated color-based thresholding algorithm in the Stereo Investigator software. The area of CD68-positive cortex was expressed as a percentage of total cortex.

For each experiment, the corresponding statistics test is indicated in the figure legend. Number of samples for each group is always shown in the figure. Statistical analysis was performed by using GraphPad Prism Version 7.0 (GraphPad Software, La Jolla, CA, USA). Values were presented as mean ± SEM. Statistical significance was determined using Student's t test and analysis of variance (ANOVA), followed by Bonferroni's, Dunnet's, or Sidak's post hoc testing as appropriate.

Neuron, Volume *95*

Supplemental Information

TDP-43 Depletion in Microglia Promotes Amyloid Clearance but Also Induces Synapse Loss

Rosa C. Paolicelli, Ali Jawaid, Christopher M. Henstridge, Andrea Valeri, Mario Merlini, John L. Robinson, Edward B. Lee, Jamie Rose, Stanley Appel, Virginia M.-Y. Lee, John Q. Trojanowski, Tara Spires-Jones, Paul E. Schulz, and Lawrence Rajendran

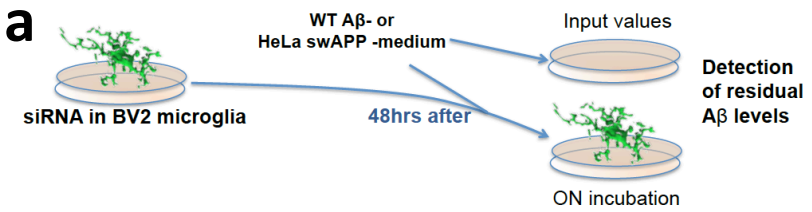

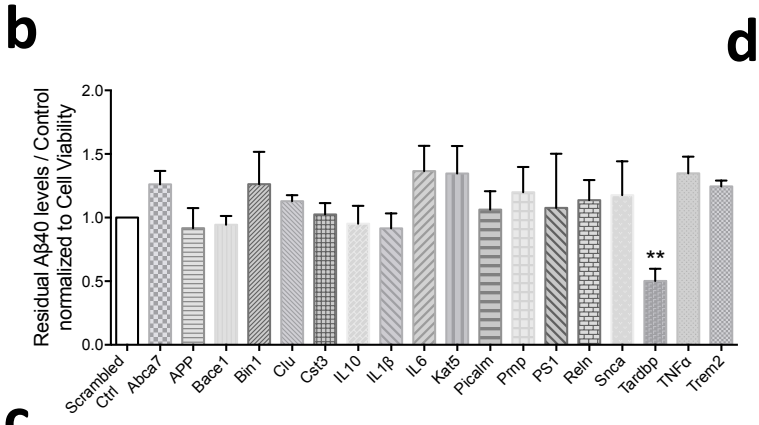

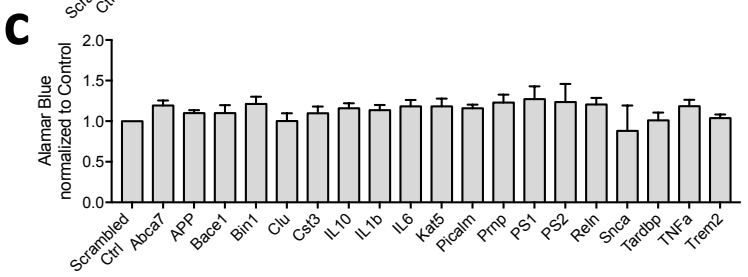

d

Number of families	1				
Number of comparisons per family	18				
Alpha	0.05				
Uncorrected Fisher's LSD	Mean Diff.	95.00% CI of diff.	Significant?	Summary	Individual P Value
Scrambled Ctrl vs. Abca7	-0.2612	-0.631 to 0.1085	No	ns	0.1632
Scrambled Ctrl vs. APP	0.0827	-0.3701 to 0.5355	No	ns	0.7168
Scrambled Ctrl vs. Bace1	0.05565	-0.4672 to 0.5785	No	ns	0.8325
Scrambled Ctrl vs. Bin1	-0.2632	-0.6766 to 0.1502	No	ns	0.2083
Scrambled Ctrl vs. Clu	-0.1291	-0.4988 to 0.2406	No	ns	0.4885
Scrambled Ctrl vs. Cst3	-0.02469	-0.3944 to 0.345	No	ns	0.8944
Scrambled Ctrl vs. IL10	0.04823	-0.3395 to 0.436	No	ns	0.8048
Scrambled Ctrl vs. IL1β	0.08454	-0.2852 to 0.4543	No	ns	0.6498
Scrambled Ctrl vs. IL6	-0.366	-0.7794 to 0.04736	No	ns	0.0818
Scrambled Ctrl vs. Kat5	-0.3468	-0.7346 to 0.04098	No	ns	0.0788
Scrambled Ctrl vs. Picalm	-0.06281	-0.4325 to 0.3069	No	ns	0.7358
Scrambled Ctrl vs. Prnp	-0.1992	-0.5689 to 0.1705	No	ns	0.2862
Scrambled Ctrl vs. PS1	-0.07573	-0.5986 to 0.4471	No	ns	0.7735
Scrambled Ctrl vs. Reln	-0.1371	-0.5504 to 0.2763	No	ns	0.5106
Scrambled Ctrl vs. Snca	-0.1762	-0.6991 to 0.3466	No	ns	0.5037
Scrambled Ctrl vs. Tardbp	0.4993	0.1295 to 0.869	Yes	**	0.0088
Scrambled Ctrl vs. TNFα	-0.348	-0.7177 to 0.02174	No	ns	0.0647
Scrambled Ctrl vs. Trem2	-0.2454	-0.6588 to 0.1679	No	ns	0.2404

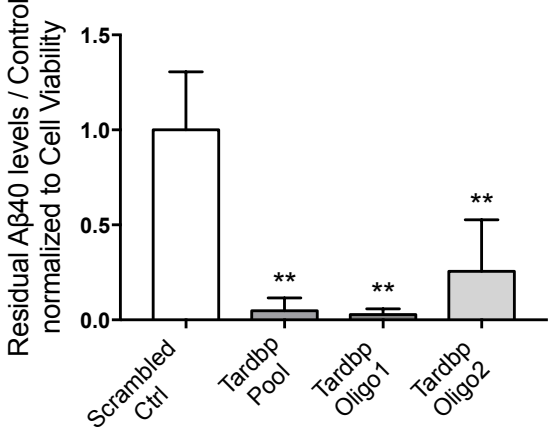

Supplementary Figure 1

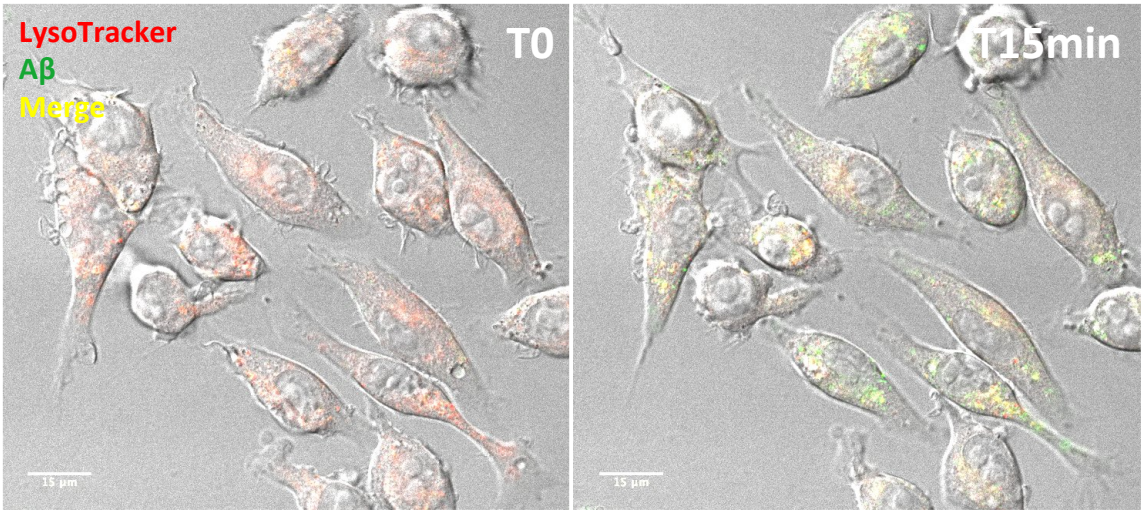

Supplementary Figure 2

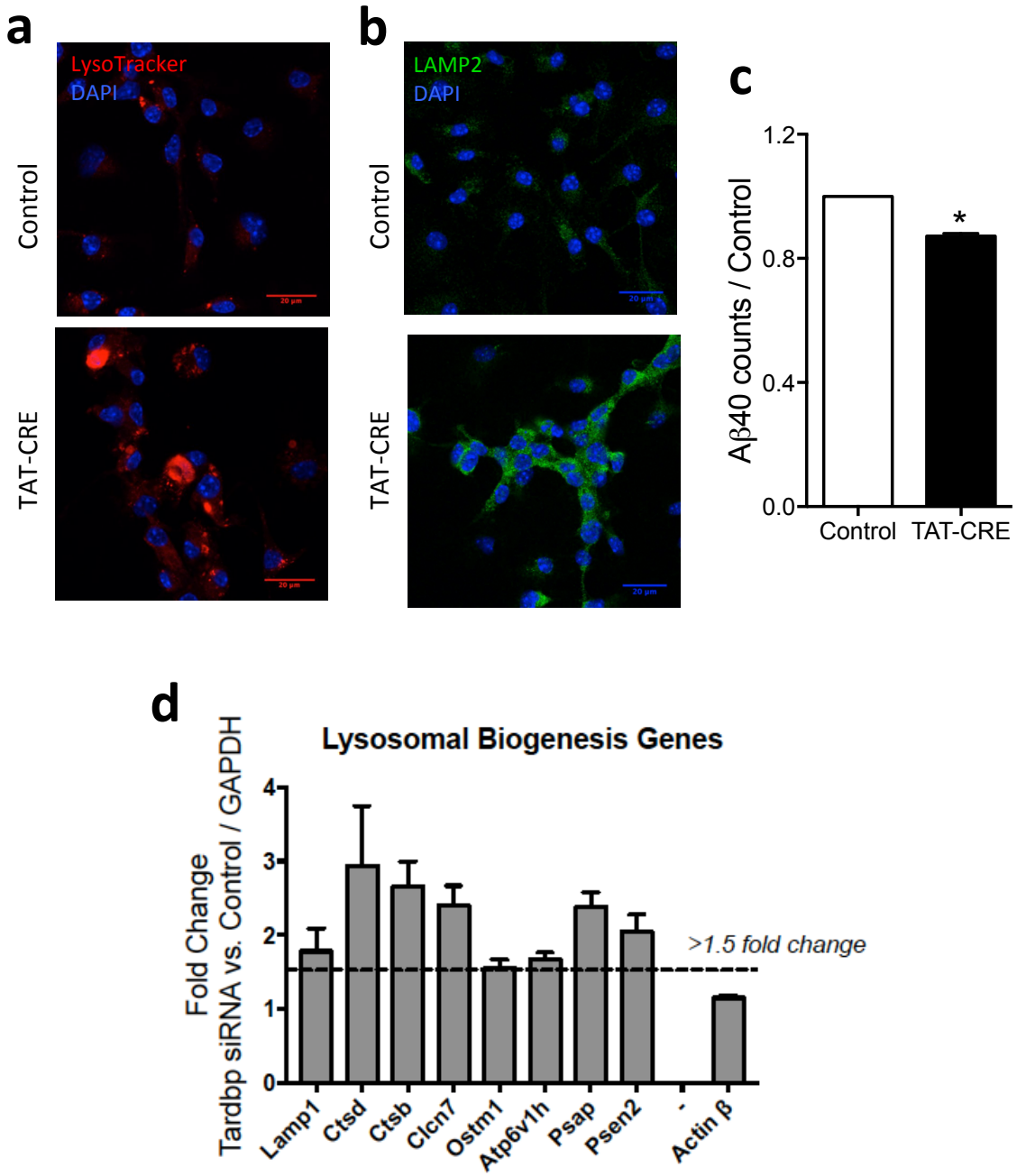

Supplementary Figure 3

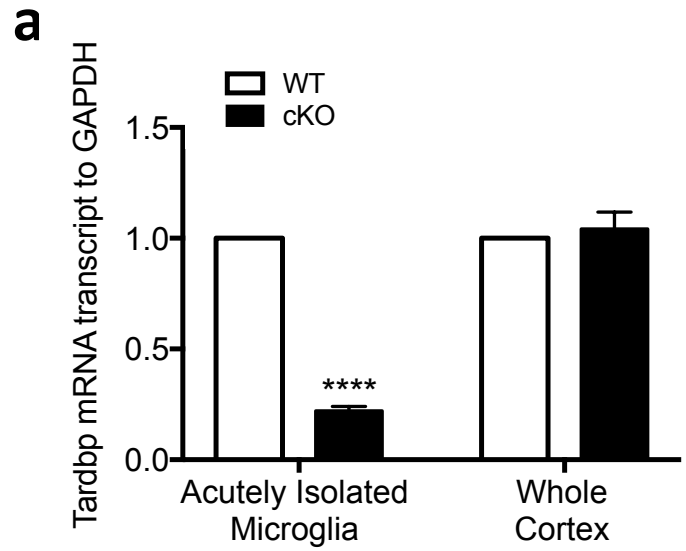

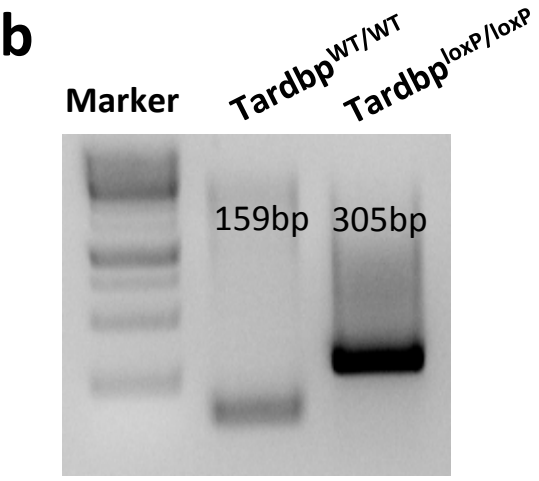

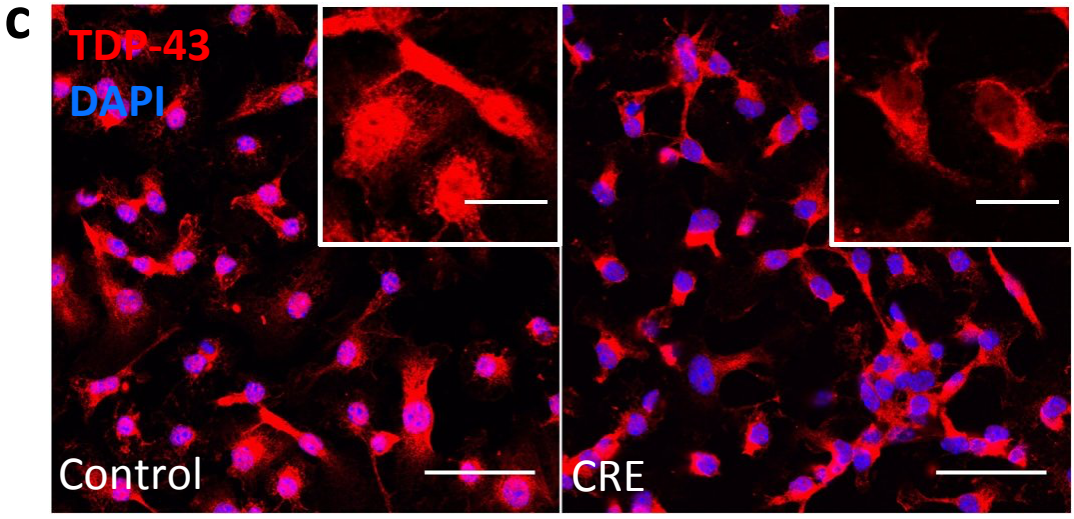

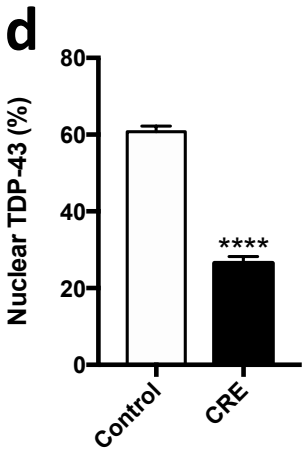

Supplementary Figure 4

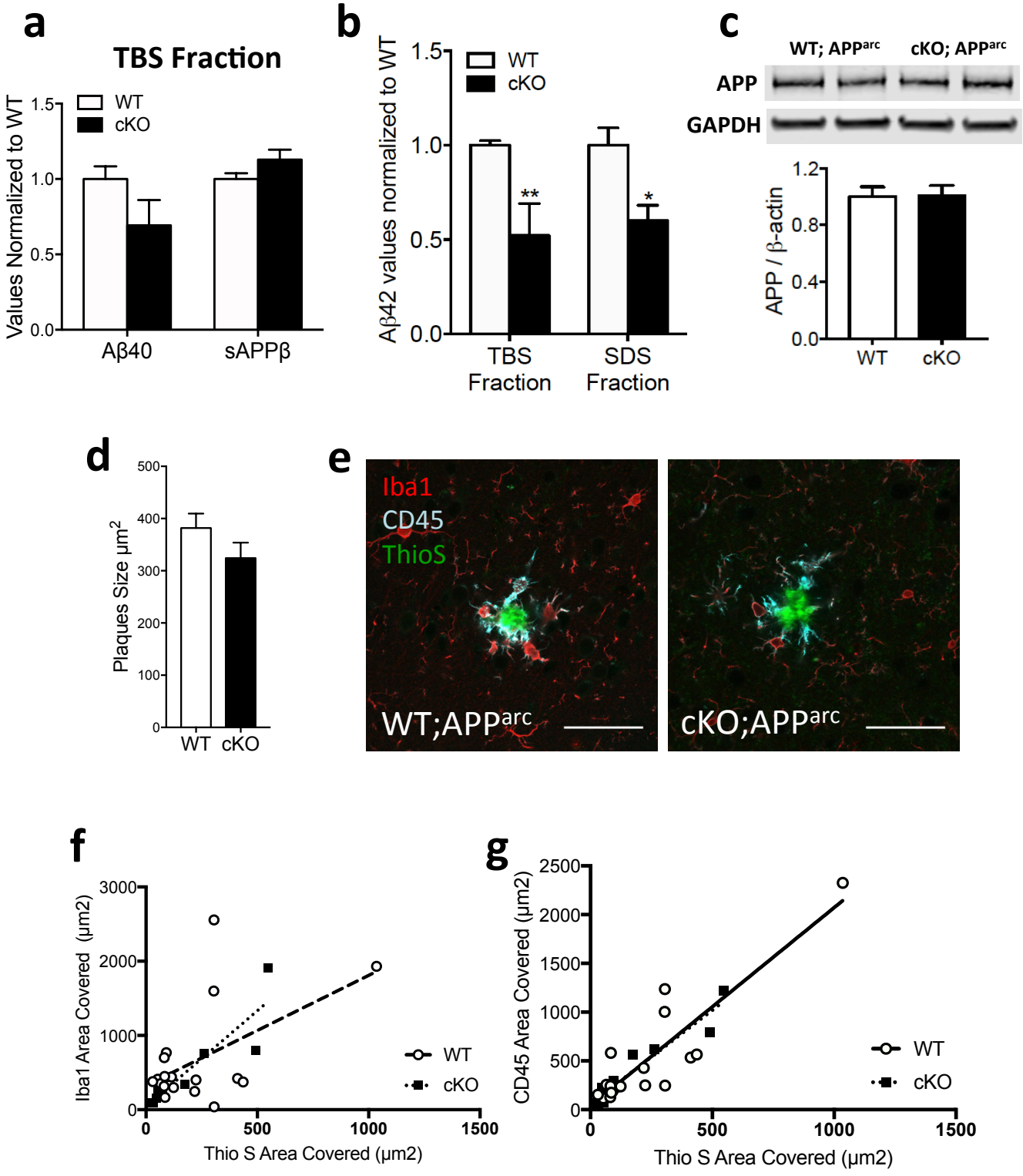

Supplementary Figure 5

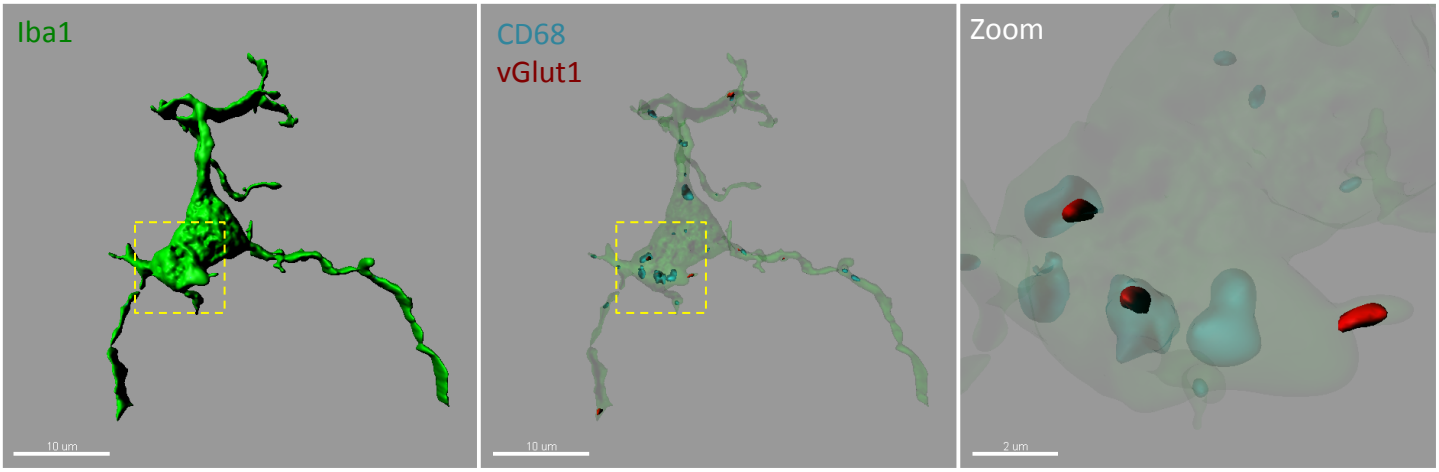

Supplementary Figure 6

Supplementary Figures Legends

Figure S1, related to Figure 1. Screen and identification of Tardbp

a, Aβ clearance assay in BV2 cells: the clearance capacity of microglia was measured by their capability to clear murine Aβ upon overnight incubation with WT primary neurons-conditioned medium. **b**, Knockdown screen for 18 genes associated with neurodegenerative disorders, assessed in Aβ clearance assay: residual murine WT Aβ levels were significantly reduced in Tardbp depleted cells compared to scrambled control (n=3-6, mean±sem ** $p<0.01$, one-way ANOVA, Uncorrected Fisher's LSD Test). **c**, cell viability assay ensuring no toxic effects due to genes knockdown. **d**, table reporting the p value for each comparison vs. control (n=3-6, mean±sem ** $p<0.01$, one-way ANOVA, Uncorrected Fisher's LSD Test).
e, Residual Aβ40 levels from HeLa swAPP conditioned medium, after overnight incubation with BV2 cells depleted of TDP-43, normalized to scrambled control and to cell viability (means±SEM, ** $p<0.005$, using one-way ANOVA followed by Dunnett's multiple comparison test).

Figure S2, related to Figure 1. Internalized Aβ colocalize with acidic vesicles

a, Representative confocal image of BV2 cells at T0 and after 15min incubation with pH sensitive dye LysoTracker (red) and fluorescently-labeled Aβ40 (green). Co-localization of the signals upon internalization is shown in yellow.

Figure S3, related to Figure 1. TDP-43 depletion promotes lysosomal biogenesis

a, Representative single focal plane micrographs for LysoTracker staining and **b**, immunohistochemistry against LAMP2 in $Tardbp^{floxed/floxed}$ primary microglia treated with control glycerol solution or recombinant CRE enzyme.

c, Quantification of Aβ clearance assay in control- or CRE-treated $Tardbp^{floxed/floxed}$ primary microglia, showing significant reduction in residual $A\beta_{40}$Swe levels normalized to control (mean±SEM, n=2; *p<0.05, using two-tailed unpaired t-test). **d**, Fold-change expression of TFEB-regulated genes in BV2 cells depleted of TDP-43, as compared to scrambled control, normalized to GAPDH reference gene (>1.5 fold change cutoff, mean±SEM, n=2)

Figure S4, related to Figure 2. Validation of microglial TDP-43 depletion in Tardbp floxed mice

a, RT-PCR detection of Tardbp mRNA transcripts normalized to Gapdh reference gene in an acutely isolated microglia population (pool of 4 brains per experiment, n=2 or in whole cortex from WT (n=3) or cKO (n=3) mice. ****p<0.0001 by two-way ANOVA, followed by uncorrected Fisher's LSD test. **b**, PCR from genomic DNA extracted by acutely isolated microglia confirming the presence of floxed Tardbp sequence in cKO samples compared to WT. **c**, Representative single focal plane micrographs for TDP-43 immunopositive signal, in control- or CRE-treated $Tardbp^{floxed/floxed}$ primary microglia. Scale bar, 40µm. Inset, scale bar, 15µm. **d**, Quantification of nuclear TDP-43 signal, shown as percentage of the nuclear area, in control- (n=200) or CRE-treated (n=173) $Tardbp^{floxed/floxed}$ primary microglia (mean±SEM, n=3 per treatment, ****p<0.0001, using two-tailed unpaired t-test).

Figure S5, related to Figure 3. Reduced amyloid levels in cKO mice

Multiplexed electrochemoluminescent ELISA measurement of **a**, Aβ40 and sAPPβ levels in the TBS-fraction from App^{arc};WT and cKO cortex homogenates (mean±SEM, n=4 mice per genotype) and **b**, Aβ42 levels in the TBS- and SDS-fraction of the same samples (mean±SEM, **p<0.01, *p<0.05, by two-way ANOVA, followed by uncorrected Fisher's LSD test). **c**, Representative western blots for APP detection in cortex of App^{arc};WT and cKO mice, and relative quantification (mean±SEM, n=4 mice per genotype). **d**, Quantification of plaque size in the cortex of App^{arc};WT and KO mice (WT n=158, cKO n=73 plaques) **e**, Representative max-projections of confocal stacks, acquired from cortex of WT;APP^{arc} or cKO;APP^{arc} adult mice, stained for amyloid plaques (ThioS) and immunostained for microglia markers (Iba1, CD45). Scale bar, 50µm. **f,** Positive correlation between plaque size/ThioS and Iba1 or **g**, plaque size/ThioS and CD45 staining is not different between genotypes, as shown by linear regression analysis. Mean±SEM, WT n=18, cKO n=10 plaques; 4 animals per genotype.

Figure S6, related to Figure 4. Engulfment of synaptic markers by microglia

Representative 3D reconstruction of a single microglia cell acquired by confocal microscopy from the somatosensory cortex of a $Cx3cr1^{CreER}$;$Tardbp^{+/+}$ mouse. The reconstruction shows vGlut1 immunoreactive puncta localized within CD68-positive phagocytic structure, inside an Iba1-positive microglia.

Supplementary Table 1, related to Figure 5a,b
Detailed information related to the ALS cohort selected for the clinical study.

	ALS (65-74 yrs)			ALS (≥75 yrs)		
	with AD (n=25)	without AD (n=505)	p value	with AD (n=12)	without AD (n=156)	p value
Gender % male	48	59.8	0.167	83.3	48.7	0.02*
Race % Caucasian	88	91.7	0.496	91.7	94.9	0.677
ApoE genotype % ApoE4 (3/4, 4/4)	45.5	28	0.132	16.7	22.4	0.232
Type of symptom onset % Bulbar	56	33.7	0.067#	50	41.9	0.4
Survival in years mean±SD	1.97±0.801	2.91±1.635	0.134	3.04±2.52	2.59±1.94	0.57
MMSE mean±SD	26.5±0.58	27.38±2.86	0.542	22.5±0.71	26.15±2.29	0.135
Years of education mean±SD	15.8±1.56	14.16±0.19	0.22	14±2.00	13.26±0.48	0.70

Supplementary Table 2, related to Figure 5e-g
Detailed information related to the human post-mortem samples used for CD68, and pTDP-43-Iba1 colocalization study.

Edinburgh Brain Bank Identifier	MRC Unique Identifier	Diagnosis	Age	Sex
SD001-16	BBN001.28406	Healthy Control	79	M
SD017-16	BBN001.28793	Healthy Control	79	F
SD018-16	BBN001.28794	Healthy Control	79	F
SD024-15	BBN001.26495	Healthy Control	78	M
SD051-15	BBN001.28402	Healthy Control	79	M
SD063-13	BBN_19686	Healthy Control	77	F
SD002-16	BBN001.28407	ALS	67	F
SD004-16	BBN001.28409	ALS	62	F
SD010-14	BBN_20604	ALS	62	F
SD014-14	BBN_20613	ALS	50	M
SD016-14	BBN_20993	ALS	43	M
SD018-15	BBN_25742	ALS	58	M
SD021-15	BBN_26494	ALS	60	M
SD026-15	BBN001.26125	ALS	49	F
SD027-14	BBN_22225	ALS	62	M
SD027-15	BBN001.26126	ALS	71	M
SD029-15	BBN001.26098	ALS	59	F
SD030-15	BBN001.26128	ALS	74	M
SD033-15	BBN001.26497	ALS	63	F
SD036-15	BBN001.26498	ALS	78	M
SD041-14	BBN_24218	ALS	68	M
SD045-15	BBN001.26729	ALS	83	F
SD046-15	BBN001.26730	ALS	54	M
SD047-13	BBN_18803	ALS	75	F
SD048-14	BBN_24321	ALS	63	F
SD049-13	BBN_18806	ALS	60	M
SD049-15	BBN001.26765	ALS	66	F
SD052-13	BBN_18807	ALS	65	F
SD053-13	BBN_19689	ALS	89	M
SD057-13	BBN_19688	ALS	57	M
SD058-13	BBN_20616	ALS	40	F
SD059-13	BBN_20617	ALS	71	M
SD059-14	BBN_24669	ALS	64	M